ICARUS/TM-2001/10
December 21, 2001

On the energy and baseline optimization to study effects related to the δ-phase (CP-/T-violation) in neutrino oscillations at a Neutrino Factory

A. Bueno[1], M. Campanelli[2], S. Navas-Concha[3] and A. Rubbia[4]

Institut für Teilchenphysik, ETHZ, CH-8093 Zürich, Switzerland

Abstract

In this paper we discuss the detection of CP and T-violation effects in the framework of a neutrino factory. We introduce three quantities, which are good discriminants for a non vanishing complex phase (δ) in the 3×3 neutrino mixing matrix: Δ_δ, Δ_{CP} and Δ_T. We find that these three discriminants (in vacuum) all scale with L/E_ν, where L is the baseline and E_ν the neutrino energy. Matter effects modify the scaling, but these effects are large enough to spoil the sensitivity only for baselines larger than 5000 km. So, in the hypothesis of constant neutrino factory power (i.e. number of muons inversely proportional to muon energy), the sensitivity on the δ-phase is independent of the baseline chosen. Specially interesting is the direct measurement of T-violation from the "wrong-sign" electron channel (i.e. the Δ_T discriminant), which involves a comparison of the $\nu_e \to \nu_\mu$ and $\nu_\mu \to \nu_e$ oscillation rates. However, the $\nu_\mu \to \nu_e$ measurement requires magnetic discrimination of the electron charge, experimentally very challenging in a neutrino detector. Since the direction of the electron curvature has to be estimated before the start of the electromagnetic shower, low-energy neutrino beams and hence short baselines, are preferred. In this paper we show, as an example, the exclusion regions in the $\Delta m^2_{12} - \delta$ plane using the Δ_{CP} and Δ_T discriminants for two concrete cases keeping the same L/E_ν ratio (730 km/ 7.5 GeV and 2900 km/30 GeV). We obtain a similar excluded region provided that the electron detection efficiency is $\sim$20% and the charge confusion 0.1%. The Δm^2_{12} compatible with the LMA solar data can be tested with a flux of $5{\times}10^{21}$ muons. We compare these results with the fit of the visible energy distributions.

[1]Antonio.Bueno@cern.ch
[2]Mario.Campanelli@cern.ch
[3]Sergio.Navas.Concha@cern.ch
[4]Andre.Rubbia@cern.ch

1 Introduction

The firmly established disappearance of muon neutrinos of cosmic ray origin [1] strongly points toward the existence of neutrino oscillations [2].

The first generation long baseline (LBL) experiments — K2K [3], MINOS [4], OPERA [5] and ICARUS [6, 7, 8] — will search for a conclusive and unambiguous signature of the oscillation mechanism using artificial neutrino beams produced by the "traditional" meson-decay method. They will provide the first precise measurements of the parameters governing the main muon disappearance mechanism.

In contrast, a neutrino factory[9, 14] is understood as a machine where low energy muons of a given charge are accelerated in a storage ring. Neutrino factories raised the interest of the physics community, since they appear natural follow-ups to the current experimental LBL program and could open the way to future muon colliders.

The real physics potential of a neutrino factory comes from its ability to test in a very clean and high statistics environment all possible flavor oscillation transitions. As many studies have shown [10], the physics potential of such facilities are very vast. An entry-level neutrino factory could test the LSND signal in a background free environment[11]. A neutrino factory source would be of sufficiently high intensity to perform very long baseline (transcontinental) experiments.

The ability to measure all possible neutrino oscillations will provide very stringent information on all the elements of the neutrino mixing matrix and on the mass pattern of the neutrinos. In a 3×3-mixing scenario, the mixing matrix, which should be unitary, is determined by three angles and a complex phase. As studies have shown [10], precise determination of two angles and of the largest mass difference will be obtained. In addition, a test of the unitarity of the matrix could be performed.

Apart from being able to measure very precisely all the magnitude of the elements of the mixing matrix, the more challenging and most interesting goal of the neutrino factory will be the search for effects related to the complex phase of the mixing matrix. The complex phase will in general alter the neutrino flavor oscillation probabilities, and will most strikingly introduce a difference of transition probabilities between neutrinos and antineutrinos (so called CP-violation effects), and between time-reversed transitions (so called T-violation effects)[20]. Neutrino factories should provide the intense and well controlled beams needed to perform these studies.

Two fundamental experimental parameters for these studies are (1) the energy E_μ of the stored muon beam which determines the neutrino energy E_ν spectrum and (2) the baseline L between the source and the detector. In earlier works, one has advocated high energy neutrinos, with a consensus around $E_\mu \simeq 30 - 50$ GeV coupled to long baselines $L \simeq 3000$ km. In Ref.[21], a much lower muon energy in the range $E_\mu \simeq 1$ GeV coupled to short baselines $L \simeq 100$ km has been proposed. This apparent contradiction was recently addressed by Lipari[16].

In this paper, we expand our early work[17] on the detection of CP-violation at a neutrino factory. In particular, we concentrate on the general strategies to detect effects related to the complex phase of the neutrino mixing matrix. The complete and comprehensive detection of the effect is very difficult for terrestrial experiments, as it would require L/E_ν values simultaneously in the range of solar and atmospheric neutrinos. We concentrate on medium L/E_ν and demonstrate that the relevant effects scales as L/E_ν and that there is an optimal choice for the ratio L/E_ν, given by the neutrino mass pattern. Hence this yields an priori large freedom for the choice of L and E_ν. We show however that for too large L, matter effects destroy the sensitivity to the complex phase, so baselines smaller than $L \simeq 5000$ km are preferred. In addition, owing to the linear rise of the neutrino cross-section with neutrino energy at high energy, the statistical significance of the effect scales with E_ν, and hence grows linearly with L, for L/E_ν constant.

The choice of baseline L is particularly critical, in the sense that at the time that a neutrino factory would start running, there will be already existing experiments at baselines from 730 km from FNAL and CERN: (1) at Soudan, MINOS with its 5.4 kton fiducial mass will have been fully operational, and similarly, (2) at GranSasso, the OPERA experiment and a multi-kton ICARUS detector. In view of the existence of such massive devices, it is worth considering if these detectors at their current baselines could be reused or improved in the context of the neutrino factory. If new sites have to be found in order to satisfy the requirements of longer baselines, major new "investments" will be required.

As far as the neutrino energy is concerned, it is clear that the average neutrino energy E_ν scales linearly with the muon beam energy E_μ. A non-negligible aspect of the neutrino factory is the need to accelerate quickly the muons to the desired energy, and so, it is expected that higher energies will be more demanding that lower ones. Eventually, cost arguments could determine the muon energy. It could therefore be that lower energy, more intense neutrino factories could be more advantageous than higher energy, less intense ones.

2 The effects related to δ in vacuum

In a three-family neutrino oscillation scenario, the flavor eigenstates $\nu_\alpha (\alpha = e, \mu, \tau)$ are related to the mass eigenstates $\nu'_i (i = 1, 2, 3)$ by the mixing matrix U

$$\nu_\alpha = U_{\alpha i} \nu'_i \tag{1}$$

and it is customary to parameterize it as:

$$U(\theta_{12}, \theta_{13}, \theta_{23}, \delta) = \begin{pmatrix} c_{12}c_{13} & s_{12}c_{13} & s_{13}e^{-i\delta} \\ -s_{12}c_{23} - c_{12}s_{13}s_{23}e^{i\delta} & c_{12}c_{23} - s_{12}s_{13}s_{23}e^{i\delta} & c_{13}s_{23} \\ s_{12}s_{23} - c_{12}s_{13}c_{23}e^{i\delta} & -c_{12}s_{23} - s_{12}s_{13}c_{23}e^{i\delta} & c_{13}c_{23} \end{pmatrix} \tag{2}$$

with $s_{ij} = \sin\theta_{ij}$ and $c_{ij} = \cos\theta_{ij}$.

We adopt the usual neutrino mass assignment in which the smallest $\Delta m^2_{21} \equiv m^2_2 - m^2_1$ is assigned to the solar neutrino deficit and the largest mass difference, $\Delta m^2_{31} \approx \Delta m^2_{32}$ is describing the atmospheric neutrino observations. We neglect accordingly the important results from LSND, awaiting further clarification from the MiniBOONE experiment. We therefore consider the following indicative set of oscillation parameters[1], compatible with current experimental observations (neglecting the LSND claim):

$$\Delta m^2_{32} = 3 \times 10^{-3}\mathrm{eV}^2, \quad \sin^2\theta_{23} = 0.5 \tag{3}$$

The value of the angle θ_{13} is currently not known, and the best experimental bound comes from CHOOZ[12] which limits $\sin^2 2\theta_{13} \lesssim 0.1$. We take:

$$\sin^2 2\theta_{13} = 0.05 \tag{4}$$

For the solar parameters, we assume values compatible with the LMA-solution, which is known to yield optimal conditions for CP-violation studies (see Ref. [13]):

$$\Delta m^2_{21} = 1 \times 10^{-4}\mathrm{eV}^2, \quad \sin^2\theta_{12} = 0.5 \tag{5}$$

With this mass assignment and with the parameterization of the mixing matrix described above, a neutrino factory can provide precise information on the largest squared mass difference $\Delta m^2_{13} \approx \Delta m^2_{23}$ and on both angles θ_{23} and θ_{13}.

In the case where neutrinos (or antineutrinos) propagate in vacuum, the probability for flavor transition has a simple behavior. It can be written as

$$P(\nu_\alpha \rightsquigarrow \nu_\beta; E_\nu, L) \;\; = \;\; \sum_{jk} J_{\alpha\beta jk} e^{-i\Delta m^2_{jk} L/2E} \tag{6}$$

where E_ν is the neutrino energy and L the baseline between the source and the detector. The Jarlskog factor is $J_{\alpha\beta jk} = U_{\beta j} U^*_{\beta k} U^*_{\alpha j} U_{\alpha k}$. For antineutrinos, we must replace $U \to U^*$, i.e. $J_{\alpha\beta jk} \to J^*_{\alpha\beta jk} = J_{\alpha\beta kj} = J_{\beta\alpha jk}$.

Since in general we have $J_{\alpha\beta jk} \neq J^*_{\alpha\beta jk}$, the probability for neutrinos $P(\nu_\alpha \to \nu_\beta; E_\nu, L)$ can be different from that for anti-neutrinos $P(\bar\nu_\alpha \to \bar\nu_\beta; E_\nu, L)$, leading to the CP-violating effects. Since $J_{\alpha\beta jk} = J^*_{\beta\alpha jk}$, there are also T-violating effects. From the definition of J also follows that (CPT-invariance)

$$P(\nu_\alpha \rightsquigarrow \nu_\beta; E_\nu, L) = P(\bar\nu_\beta \rightsquigarrow \bar\nu_\alpha; E_\nu, L) \tag{7}$$

[1]Note that in studies of effects related to δ, the signs of the Δm^2's are important.

The oscillation probability can be made more explicit by separating real and imaginary contributions of $J_{\alpha\beta jk}$:

$$\begin{aligned} P(\nu_\alpha \rightsquigarrow \nu_\beta; E_\nu, L) &= \sum_j J_{\alpha\beta jj} + \sum_{j>k} \left(J_{\alpha\beta jk} e^{-i\Delta m^2_{jk} t/2E} + J^*_{\alpha\beta jk} e^{+i\Delta m^2_{jk} t/2E} \right) \quad (8) \\ &= \delta_{\alpha\beta} - 4 \sum_{j>k} \Re e J_{\alpha\beta jk} \sin^2(\Delta_{jk}) \quad (9) \\ &\quad + 4 \sum_{j>k} \Im m J_{\alpha\beta jk} \sin(\Delta_{jk}) \cos(\Delta_{jk}) \end{aligned}$$

Here

$$\Delta_{jk} \equiv \Delta m^2_{jk} \frac{L}{4E_\nu} \quad (10)$$

and $\Delta_{12} + \Delta_{23} + \Delta_{31} = 0$. For anti-neutrinos, we must replace $\Im m J_{\alpha\beta jk} \to -\Im m J_{\alpha\beta jk}$. Hence, the first two terms of P form a CP-even term, and the last one is a CP-odd term.

In the rest of the paper, we concentrate on transitions between electron and muon neutrinos. One can explicitly calculate the probabilities, inserting the elements of the chosen mixing matrix parameterization:

$$\begin{aligned} & P(\nu_e \to \nu_\mu) = P(\bar\nu_\mu \to \bar\nu_e) = \\ & 4c^2_{13} \left[\sin^2\Delta_{23} s^2_{12} s^2_{13} s^2_{23} + c^2_{12} \left(\sin^2\Delta_{13} s^2_{13} s^2_{23} + \sin^2\Delta_{12} s^2_{12} \left(1 - \left(1 + s^2_{13} \right) s^2_{23} \right) \right) \right] \\ & - \frac{1}{2} c^2_{13} \sin(2\theta_{12}) s_{13} \sin(2\theta_{23}) \, \underline{\cos\delta} \left[\cos 2\Delta_{13} - \cos 2\Delta_{23} - 2\cos(2\theta_{12}) \sin^2\Delta_{12} \right] \\ & + \frac{1}{2} c^2_{13} \, \underline{\sin\delta} \sin(2\theta_{12}) s_{13} \sin(2\theta_{23}) \left[\sin 2\Delta_{12} - \sin 2\Delta_{13} + \sin 2\Delta_{23} \right] \quad (11) \end{aligned}$$

This expression has been split in a first part independent from the phase δ, and in the two parts proportional respectively to $\cos\delta$ and $\sin\delta$. To obtain the probabilities for $\nu_\mu \to \nu_e$ and $\bar\nu_e \to \bar\nu_\mu$, we must replace $\delta \longrightarrow -\delta$, with the effect of changing $\sin\delta \longrightarrow -\sin\delta$ and $\cos\delta \longrightarrow \cos\delta$. The term proportional to $\sin\delta$ is the CP- or T-violating term, while the $\cos\delta$ term equally modifies the probability for both CP-conjugate states.

The behavior in the range where the energy is too large or the baseline too short to be sensitive to the smallest mass difference, i.e. $|\Delta m^2_{12}| \ll E_\nu/L$ or $|\Delta_{12}| \ll 1$, is found by $\Delta_{12} \to 0$ and $\Delta_{13} \to \Delta_{23}$. Both terms depending on $\cos\delta$ and $\sin\delta$ vanish, and we recover the well known probability

$$P(\nu_e \to \nu_\mu) \simeq \sin^2(2\theta_{13}) s^2_{23} \sin^2(\Delta_{23}) \quad (12)$$

Going back to the general case, the $\nu_e \to \nu_\mu$ oscillation probability can be simplified by introducing values for θ_{12} and θ_{23} consistent with current experimental knowledge.

Indeed, for $\theta_{12} = \theta_{23} = \pi/4$, we find

$$P(\nu_e \to \nu_\mu) = \frac{1}{2} c_{13}^2 \Big\{ c_{13}^2 \sin^2 \Delta_{12} + s_{13} \Big[2 \sin \Delta_{12} \sin(\Delta_{13} + \Delta_{23} - \delta) + \sin \delta \sin 2\Delta_{12} + 2 s_{13} \left(\sin^2 \Delta_{13} + \sin^2 \Delta_{23} \right) \Big] \Big\} \quad (13)$$

From this dependence, we see that a precise measurement of the $\nu_e \to \nu_\mu$ oscillation probability can yield information of the δ-phase provided that the other oscillation parameters in the expression are known sufficiently accurately. We also note that the phase δ changes the neutrino energy position of the maximum of the oscillation, because of the term $\sin(\Delta_{13} + \Delta_{23} - \delta)$.

Clearly, the dependence of the parameter δ is a priori most "visible" in the energy-baseline range such that $|\Delta_{12}| = |\Delta m^2_{21}| L/4E_\nu \simeq 1$ and $|\Delta_{23}| = |\Delta m^2_{23}| L/4E_\nu \simeq 1$. This is the region where all terms in Eq. (13) contribute.

When $|\Delta_{12}| \ll 1$ and $|\Delta_{23}| \simeq 1$, we obtain

$$P(\nu_e \to \nu_\mu) \simeq \frac{1}{2} c_{13}^2 \Big\{ c_{13}^2 \Delta_{12}^2 + 2 s_{13}^2 \left(\sin^2 \Delta_{13} + \sin^2 \Delta_{23} \right) + 2 \Delta_{12} s_{13} \Big[\sin(\Delta_{13} + \Delta_{23}) \cos \delta + (1 - \cos(\Delta_{13} + \Delta_{23})) \sin \delta \Big] \Big\} \quad (14)$$

At even higher E_ν or smaller L, we further have, when both $|\Delta_{12}| \ll 1$ and $|\Delta_{13}|, |\Delta_{23}| \ll 1$:

$$P(\nu_e \to \nu_\mu) \simeq \frac{1}{2} c_{13}^2 \Big\{ c_{13}^2 \Delta_{12}^2 + 2 s_{13}^2 \left(\Delta_{13}^2 + \Delta_{23}^2 \right) + 2 \Delta_{12} s_{13} (\Delta_{13} + \Delta_{23}) \cos \delta \Big\} \quad (15)$$

and the dependence on the phase is only through $\cos \delta$. From this follows a degeneracy under the change of sign of δ, as was pointed out in Ref. [16]. So, in this L and E_ν range, a precise determination of the oscillation probability can no longer determine the sign of δ.

The behavior for the two baselines $L = 730$ km and 2900 km as a function of neutrino energy E_ν is explicitly shown in Figure 1. The probabilities are computed for three values of the δ-phase: $\delta = 0$ (line), $\delta = +\pi/2$ (dashed), $\delta = -\pi/2$ (dotted). The other oscillation parameters are those described in Eqs. 3 and 5: $\Delta m^2_{32} = 3 \times 10^{-3}$ eV^2, $\Delta m^2_{21} = 1 \times 10^{-4}$ eV^2, $\sin^2 \theta_{23} = 0.5$, $\sin^2 \theta_{12} = 0.5$, and $\sin^2 2\theta_{13} = 0.05$.

A region corresponding to the oscillation of the "first maximum" is clearly visible on the curves. We define the energy of the "first maximum" as follows

$$\Delta_{32} = \frac{\pi}{2} \longrightarrow E_\nu^{max} \equiv \frac{\Delta m^2_{32}}{2\pi} L$$
$$\longrightarrow E_\nu^{max}(\mathrm{GeV}) \simeq \Delta \mathrm{m}^2_{32}(\mathrm{eV}^2) \left(\frac{2 \times 1.27}{\pi} \right) \mathrm{L(km)} \quad (16)$$

which yields $E_\nu^{max} \simeq 2$ GeV at 730 km, $E_\nu^{max} \simeq 8$ GeV at 2900 km and $E_\nu^{max} \simeq 20$ GeV at 7400 km for $\Delta m^2_{32} = 3\times 10^{-3}$ eV^2. This energy corresponds to the point of maximum oscillation induced by Δm^2_{32} and coincides with the maximum when $\delta = 0$. It will be useful when we discuss the point of maximum sensitivity to the δ-phase.

A similar relation can also be defined in terms of L/E_ν which is

$$\left(\frac{L}{E_\nu}\right)^{max} \equiv \frac{2\pi}{\Delta m^2_{32}} \longrightarrow \left(\frac{L(\text{km})}{E_\nu(\text{GeV})}\right)^{max} \simeq \left(\frac{\pi}{2\times 1.27\Delta m^2_{32}(\text{eV}^2)}\right) \tag{17}$$

which is approximately equal $(L/E_\nu)^{max} \simeq 400$ km/GeV for $\Delta m^2_{32} = 3\times 10^{-3}$ eV^2.

The dependence at high energy is not easily understood from a plot of the probabilities as a function of energy. In addition, while the effect is expected to be most "visible" at low energies, experiments at low energy are a priori more difficult to perform than at high energy, because of the rising cross-section, easiness of detection and neutrino flux considerations. In fact, what is more important is not the probability behavior, but rather how will the number of events, observed in a given experiment at a given baseline L within a certain neutrino energy range, depend on the phase δ, relative to the total number of observed events in absence of δ phase effects. Hence, in the following, we consider for definiteness the neutrino flux of a neutrino factory and will in order to ease the comparison between various energies and baselines introduce a "rescaled" probability.

3 The neutrino factory (NF)

The decay of the muon is a very well known process. Within the Standard Model and to leading order, the neutrino energy distribution in the muon rest frame in μ^- decays is given by

$$\frac{d^2N_{\nu_\mu}}{dxd\Omega} \propto \frac{2x^2}{4\pi}[(3-2x)+(1-2x)P_\mu\cos\theta] \tag{18}$$

$$\frac{d^2N_{\bar\nu_e}}{dxd\Omega} \propto \frac{12x^2}{4\pi}[(1-x)+(1-x)P_\mu\cos\theta] \tag{19}$$

where P_μ is the average polarization of the muon beam, $x \equiv 2E_\nu/m_\mu$, and θ is the angle between the momentum vector of the neutrino and the mean angle of the muon polarization. The beam polarization can be carefully measured via the spectrum of the electrons from muon decay; thus the spectra of the two components of the neutrino beam can be known with good accuracy, and so the ratio of the fluxes reaching the far detector.

Assuming perfect focusing, an unpolarized muon beam and for very relativistic muons, the energy spectrum of neutrinos detected at small angles with respect to the muon flight direction as in the case of long baseline experiment, is given by

$$\phi_{\nu_\mu}(z) \propto 2z^2(3-2z); \qquad \phi_{\bar\nu_e}(z) \propto 12z^2(1-z) \tag{20}$$

where $z = E_\nu/E_\mu$. A key point is that angular opening of the neutrino beam will shrink due to the Lorentz boost as $\gamma^{-2} = (E_\mu/m_\mu)^{-2}$ and hence the total neutrino fluency at a far detector will increase as E_μ^2. This means that the flux can be expressed as

$$\Phi_{\nu_\mu}(E_\mu, L, z) = \frac{E_\mu}{L^2}\phi_{\nu_\mu}(z); \qquad \Phi_{\bar{\nu}_e}(E_\mu, L, z) = \frac{E_\mu}{L^2}\phi_{\bar{\nu}_e}(z) \tag{21}$$

The scaling of the neutrino event rate can be expressed as

$$N_\nu = \int_0^{E_\mu} \Phi_{\nu_\mu}(E_\mu, L, E_\nu)\, \sigma_\nu(E_\nu) dE_\nu \tag{22}$$

$$= \frac{E_\mu^2}{L^2} \int_0^1 \phi_\nu(z)\sigma_\nu(zE_\mu)dz \tag{23}$$

since $dE_\nu = E_\mu dz$. By approximating the neutrino cross-section as a linear function of the neutrino energy, i.e. $\sigma_\nu(zE_\mu) \simeq \sigma_\nu^0 \times E_\nu$, where σ_ν^0 is a constant, we obtain

$$N_\nu \simeq \frac{E_\mu^3}{L^2}\sigma_\nu^0 \int_0^1 \phi_z z dz \propto \frac{E_\mu^3}{L^2} \tag{24}$$

The integral over z is independent of E_μ and we find the known rapid growth of neutrino events with E_μ^3, characteristic of the neutrino factory.

4 The rescaled probabilities

In order to compare effects at different energies and various baselines, we define a "rescaled probability" parameter that allows a direct comparison of effects.

Since to a good approximation (when $z \lesssim 0.6$ for electron-neutrinos and always for muon-neutrinos) the neutrino energy distribution behaves like E_ν^2 (see section 3) and in addition, the neutrino flux scales like L^{-2} due to the beam divergence, we define the "rescaled probability" parameter $p(\nu_\alpha \rightsquigarrow \nu_\beta; E_\nu, L)$ as

$$p(\nu_\alpha \rightsquigarrow \nu_\beta; E_\nu, L) \equiv P(\nu_\alpha \rightsquigarrow \nu_\beta; E_\nu, L) \times \frac{E_\nu^2}{L^2} \tag{25}$$

We note that

1. it approximately correctly "weighs" the probability by the neutrino energy spectrum E_ν^2 of the neutrino factory spectrum;
2. it can be directly compared at different baselines, since it contains the L^{-2} attenuation of the neutrino flux with distance L;
3. p tends to a constant for $E_\nu \to \infty$, hence the high energy behavior can be easily studied.

We start by illustrating the behavior of the rescaled probability for $\nu_e \to \nu_\mu$ oscillations (see Eq. 15) in the case where both $|\Delta_{12}| \ll 1$ and $|\Delta_{13}|, |\Delta_{23}| \ll 1$. We note that the expression depends on the second power of the Δ_{jk}'s. The resulting $(L/E_\nu)^2$ dependence is canceled in the rescaled probability:

$$\begin{aligned} p(\nu_e \to \nu_\mu) &\simeq \frac{1}{2} c_{13}^2 \Big\{ c_{13}^2 \Delta_{12}^2 + 2 s_{13}^2 \left(\Delta_{13}^2 + \Delta_{23}^2 \right) + 2 \Delta_{12} s_{13} (\Delta_{13} + \Delta_{23}) \cos\delta \Big\} \times \frac{E_\nu^2}{L^2} \\ &\simeq \frac{1}{32} c_{13}^2 \Big\{ c_{13}^2 (\Delta m_{12}^2)^2 + 2 s_{13}^2 \Big((\Delta m_{13}^2)^2 + (\Delta m_{23}^2)^2 \Big) \\ &\quad + 8 \Delta m_{12}^2 s_{13} (\Delta m_{13}^2 + \Delta m_{23}^2) \cos\delta \Big\} \end{aligned} \tag{26}$$

As expected, the result is independent of the energy E_ν and the baseline L, and the rescaled probability "constant" is modified with a $\cos\delta$ dependent term. The sign of this term depends as expected on the sign of the Δm_{jk}^2's.

Figure 2 shows the rescaled probability for $\nu_e \to \nu_\mu$ oscillations in vacuum for three baselines $L = 730$ km (line), 2900 km (dashed) and 7400 km (dotted) as a function of neutrino energy E_ν. In this case, we chose $\delta = 0$ in order to illustrate the effect of the rescaling. The interesting oscillations at low energy driven by the interference of the Δ_{12}, Δ_{13} and Δ_{23} terms are largely "damped" by the rescaling, and the situation has dramatically changed compared to Figure 1.

We also note that the asymptotic value reached at high energy is independent of the distance L, reflecting the well-known result that the oscillated number of events is independent of distance L at high energy, since the L^2 growing of the oscillation cancels the L^{-2} attenuation of the flux with distance.

The dependence on the phase δ is illustrated in Figure 3. For $\delta = \pm\pi/2$, the $\cos\delta$ term vanishes and the probability is reduced at high energy compared to the $\delta = 0$ case. The asymptotic value reached in the high energy limit is obviously independent of the baseline and is different than that reached for $\delta = 0$. For $\delta = \pm\pi/2$, it converges to the same values when the condition for $|\Delta_{12}| \ll 1$ and $|\Delta_{13}|, |\Delta_{23}| \ll 1$ is true. This depends on the baseline L considered. For $L = 730(2900)$ km, the probabilities for $\delta = \pm\pi/2$ are indistinguishable to within 10% for $E_\nu \gtrsim 20(80)$ GeV.

5 Propagation in matter

Since neutrino factories will be associated to long baseline, it is not possible to avoid including effects associated to the neutrino propagation through the Earth matter. The simplest way to take into account these effects is to maintain the formalism developed for propagation in vacuum and to replace the mixing angles and the neutrino mass differences by "effective" values.

The general exact and precise treatment of the effects induced by the propagation through the Earth can be quite complicated, due to the a priori complexity of the

matter profile in the Earth. We will hence assume that the effects due to matter can be parameterized by one parameter, i.e. the "average" density ρ, to reproduce approximately the effect of traversing the Earth. This assumption was recently revisited in Ref. [18], where it was concluded that for a baseline of 3000 km or less, the effect of the matter profile is not important. For very long baselines like $L \approx 7400$ km, they conclude that the Earth profile is important. This however does not pose us a problem, since, as we will show below, we will not consider that baseline in the context of the searches for δ-phase-induced effects. We hence all along use the approximation of constant density.

In the case of two-neutrino oscillation, in which the mixing is driven by a single mixing angle θ, and propagating in matter of constant density ρ, it is rather easy to understand the behavior of the oscillation probability for neutrinos or antineutrinos. An important quantity for matter effects is D, defined as

$$D(E_\nu, \rho) \equiv 2\sqrt{2} G_F n_e E_\nu = 7.56 \times 10^{-5} eV^2 (\frac{\rho}{gcm^{-3}})(\frac{E_\nu}{GeV}) \equiv -D(E_{\bar{\nu}}, \rho) \tag{27}$$

where n_e is the electron density and ρ the matter density. For antineutrinos, D is replaced by $-D$.

In the case of three neutrino mixing, the situation is mathematically more complex. Approximate oscillation probabilities have been considered by perturbative expansion in the oscillation parameters[19, 20, 15]. Exact formulas have been derived[22, 23] and we make use of this formalism as implemented in Ref. [17]. For completeness, we reproduce here the expressions. The mass eigenvalues in matter M_1, M_2 and M_3 are:

$$M_1^2 = m_1^2 + \frac{A}{3} - \frac{1}{3}\sqrt{A^2 - 3B}S - \frac{\sqrt{3}}{3}\sqrt{A^2 - 3B}\sqrt{1 - S^2} \tag{28}$$

$$M_2^2 = m_1^2 + \frac{A}{3} - \frac{1}{3}\sqrt{A^2 - 3B}S + \frac{\sqrt{3}}{3}\sqrt{A^2 - 3B}\sqrt{1 - S^2} \tag{29}$$

$$M_3^2 = m_1^2 + \frac{A}{3} + \frac{2}{3}\sqrt{A^2 - 3B}S \tag{30}$$

where A, B and S are given in the Appendix of Ref. [17]. For the mixing angles in matter the analytical expressions read:

$$\sin^2\theta_{12}^m = \frac{-(M_2^4 - \alpha M_2^2 + \beta)\Delta M_{31}^2}{\Delta M_{32}^2(M_1^4 - \alpha M_1^2 + \beta) - \Delta M_{31}^2(M_2^4 - \alpha M_2^2 + \beta)} \tag{31}$$

$$\sin^2\theta_{13}^m = \frac{M_3^4 - \alpha M_3^2 + \beta}{\Delta M_{31}^2 \Delta M_{32}^2} \tag{32}$$

$$\sin^2\theta_{23}^m = \frac{G^2 s_{23}^2 + F^2 c_{23}^2 + 2GF c_{23} s_{23} c_\delta}{G^2 + F^2} \tag{33}$$

where α, β, G and F are found in the Appendix of Ref. [17], and also an expression for the δ-phase in matter, i.e. δ^m.

It can be shown that in the relevant situation in which $|\Delta m^2_{21}| \ll |\Delta m^2_{31}| \approx |\Delta m^2_{32}|$, matter effects in three-family mixing decouple to two independent two-family mixing scenarios. This is essentially because matter effects become important when the parameter $D(E_\nu, \rho)$ is similar to one of the $|\Delta m^2|$'s and hence the matter effects driven by $|\Delta m^2_{21}|$ will occur for fixed density at a very different energy E_ν than for $|\Delta m^2_{31}| \approx |\Delta m^2_{32}|$. The term $|\Delta m^2_{21}|$ (resp. $|\Delta m^2_{31}|$) will produce a MSW resonance in the θ_{12}(resp. θ_{13}) angle.

Given the energies and baselines considered, we illustrate analytically our arguments for a two-family mixing matter effect in $\nu_e \to \nu_\mu$ oscillations, in which we identify the 2-mixing angle θ with the 3-mixing θ_{13} and the mass difference squared as $|\Delta m^2_{31}| \approx |\Delta m^2_{32}|$. In the case $|\Delta_{12}| \ll |\Delta_{13}| \approx |\Delta_{23}| \approx 1$ in matter, the effective mixing angles θ^m_{23}, θ^m_{12}, θ^m_{13} and δ^m will be approximately equal to (see e.g. Figure 1 of Ref. [17]) [2]

$$\begin{aligned}
\sin^2\theta^m_{23}(D) &\simeq \sin^2\theta_{23} \\
\sin^2 2\theta^m_{12}(D) &\to \approx 0 \\
\sin^2 2\theta^m_{13}(D) &= \frac{\sin^2 2\theta_{13}}{\sin^2 2\theta_{13} + (\frac{D}{\Delta m^2_{32}} - \cos 2\theta_{13})^2} \\
&\simeq \frac{\sin^2 2\theta_{13}}{\sin^2 2\theta_{13} + \mathcal{M}^2} \\
\delta^m &\approx \delta
\end{aligned} \tag{34}$$

where $\mathcal{M} \equiv D/\Delta m^2_{32} - 1$ and, for the second line, we assume θ_{13} small. This term has the well-known MSW resonance behavior, which predicts that the effective angle $\sin^2 2\theta^m_{13}(D) \to 1$ for $D \to \Delta m^2_{32}$ (i.e. $\mathcal{M} \to 0$), no matter how small $\sin^2 2\theta_{13}$ is. The effective mass squared difference becomes

$$\Delta M^2_{32} \simeq \Delta m^2_{32}\sqrt{\sin^2 2\theta_{13} + \mathcal{M}^2} \tag{35}$$

which implies that the effective oscillation wavelength becomes very large (resp. small) close to (resp. far from) the resonance energy.

The oscillation probability at small L/E_ν (see Eq. 12) is in matter

$$\begin{aligned}
P^m(\nu_e \to \nu_\mu) &\simeq \sin^2(2\theta^m_{13}) s^2_{23} \sin^2(\Delta^m_{23}) \\
&\simeq \frac{\sin^2 2\theta_{13}}{\sin^2 2\theta_{13} + \mathcal{M}^2} s^2_{23} \sin^2\left(\Delta m^2_{32}\sqrt{\sin^2 2\theta_{13} + \mathcal{M}^2}\frac{L}{4E_\nu}\right)
\end{aligned} \tag{36}$$

In the case where the neutrino energy is at the MSW resonance (i.e. $\mathcal{M} = 0$ and $E_\nu = \mathcal{E}^{res}\cos 2\theta_{13}\Delta m^2_{32}$), the probability is approximately

$$P^m(\nu_e \to \nu_\mu) \simeq s^2_{23}\sin^2\left(\Delta m^2_{32}\sqrt{\sin^2 2\theta_{13}}\frac{L}{4\mathcal{E}^{res}\cos 2\theta_{13}\Delta m^2_{32}}\right)$$

[2] In reality, the angles $\sin^2\theta^m_{12}$ and $\sin^2\theta^m_{23}$ tend to rise slightly for $D > \Delta m^2_{32}$, because the non-vanishing Δm^2_{21} splitting removes the degeneracy between muon and tau flavors (see Ref. [17]), but we neglect this effect.

$$\simeq \quad s_{23}^2 \sin^2\left(\frac{\tan 2\theta_{13}}{4\mathcal{E}^{res}} L\right)$$
$$\simeq \quad s_{23}^2 \left(\frac{\tan 2\theta_{13}}{4\mathcal{E}^{res}}\right)^2 L^2 \tag{37}$$

where in the last line we assumed $L < \tan 2\theta_{13}/4\mathcal{E}^{res} \approx 14000$ km. In this case, the probability grows with L^2, giving rise to the enhanced oscillation probability at large distances through matter.

For neutrino energies E_ν above the resonance energy E_ν^{res}, where one can approximate $\mathcal{M}^2 > 1 \gg \sin^2 2\theta_{13}$, the probability is

$$P^m(\nu_e \to \nu_\mu) \quad \simeq \quad \frac{\sin^2 2\theta_{13}}{\mathcal{M}^2} s_{23}^2 \sin^2\left(\Delta m_{32}^2 \sqrt{\mathcal{M}^2} \frac{L}{4E_\nu}\right) \tag{38}$$

and this expression will vanish for growing $\mathcal{M}$ since the sine function will not cancel the $\mathcal{M}^2$ at the denominator. These behaviors will be rediscussed later in the context of the δ-phase dependent terms.

To summarize, there will be two specific neutrino energies of interest when neutrinos propagate through matter:

1. for $D \approx \Delta m_{32}^2$, we reach for neutrinos the MSW resonance, in which the effective mixing angle $\sin^2(2\theta_{13}^m) \approx 1$. In terms of neutrino energy, this implies

$$E_\nu^{res} \quad = \quad \frac{\cos 2\theta_{13} \Delta m_{32}^2}{2\sqrt{2} G_F n_e} = \mathcal{E}^{res} \cos 2\theta_{13} \Delta m_{32}^2$$
$$\simeq \quad \frac{1.32 \times 10^4 \cos 2\theta_{13} \Delta m_{32}^2(\mathrm{eV}^2)}{\rho(g/cm^3)} \text{ in GeV} \tag{39}$$

   where $\mathcal{E}^{res} = (2\sqrt{2} G_F n_e)^{-1}$. For density parameters ρ equal to 2.7, 3.2 and 3.7 g/cm^3 one finds $E_\nu^{res} \simeq 14.1$, 12.3 and 10.7 GeV for $\Delta m_{32}^2 = 3 \times 10^{-3}$ eV^2.

2. for $D > 2\Delta m_{32}^2$, the effective mixing angle for neutrinos is always smaller than that in vacuum, i.e. $\sin^2(2\theta_{13}^m) < \sin^2(2\theta_{13})$. In terms of neutrino energy, this is equivalent to
$$E_\nu > 2E_\nu^{res} \tag{40}$$

3. these arguments are independent of the baseline L and depend only on the matter density ρ.

In the rest of the paper, we will solve the equations numerically in order to properly introduce exact matters effects into our oscillation probabilities.

The distortion of the oscillation probabilities introduced by the propagation through matter are shown in Figures 4 and 5, where the probability for $\nu_e \to \nu_\mu$ oscillations

for two baselines $L = 730$ km and 2900 km are shown as a function of neutrino energy E_ν. For each baseline, the probabilities are computed for three values of the δ-phase: $\delta = 0$, $\delta = +\pi/2$, $\delta = -\pi/2$.

We further illustrate the behavior in matter in Figures 6, 7 and 8, where the rescaled probability for $\nu_e \to \nu_\mu$ oscillations for three baselines $L = 730$ km, 2900 km and 7400 km are shown as a function of neutrino energy E_ν. For each baseline, the probabilities are computed for neutrinos in matter, in vacuum (dotted line, same for neutrinos and antineutrinos) and for antineutrinos in matter. A phase $\delta = 0$ has been assumed.

The characteristic behavior in matter can be readily seen. At the shortest baseline, $L = 730$ km, the effect of matter is small, i.e. the probabilities are very similar to that in vacuum and the probability is simply slightly enhanced (suppressed) for neutrinos (antineutrinos). Between approximately $1 < E_\nu < 10$ GeV, the rescaled probability rises; this corresponds to the oscillation at the "first maximum" (see equation 16), which yields $E_\nu^{max} \simeq 2$ GeV for 3×10^{-3} eV^2. Above $E_\nu \simeq 10$ GeV, the rescaled probability reaches a constant.

At the middle baseline $L = 2900$ km, the effect of propagation through matter is quite visible. The resonance for neutrinos can be seen at $E_\nu^{res}(GeV) \simeq 12$ GeV, which is quite close from the "first maximum", which is now given the baseline at $E_\nu^{max} \simeq 8$ GeV (see equation 16). As expected, the probability in vacuum reaches at higher energies the same constant as for the shortest baseline $L = 730$ km. However, in matter for $E_\nu \gtrsim 2E^{res}$, the probability becomes smaller than that in vacuum. For antineutrinos, the probability tends to be suppressed by matter, but tends to the same value as that of neutrinos at high energy.

For the longest baseline $L = 7400$ km, the effect of matter is quite strong. The "first maximum" is now at $E_\nu^{max} \simeq 20$ GeV (see equation 16), but this corresponds to an energy very close to the condition for $D > 2\Delta m^2_{32}$, in which the effective mixing angle for neutrinos is smaller than that in vacuum. The probability at such large distances is therefore quite "suppressed" by matter as opposed to what it would be in vacuum.

From these discussions, it is already clear that if one wants to study oscillations in the region of the "first maximum", one should not choose a too large baseline L, otherwise, matter effects will suppress the oscillation probability. This will be further discussed in the next section.

6 Detecting the δ phase at the NF and the L/E_ν scaling

We are now ready to investigate methods to optimally look for effects related to the phase δ in neutrino oscillations. We consider that propagation of neutrinos will always occur through matter and hence use the exact numerical calculations for three family

mixing, without any approximation in the oscillation probabilities, nor in the treatment of matter effects.

In order to further study the dependence of the δ-phase, we consider the following three quantities which are good discriminators for a non-vanishing phase δ:

1. $\Delta_\delta \equiv P(\nu_e \to \nu_\mu, \delta = +\pi/2) - P(\nu_e \to \nu_\mu, \delta = 0)$
   The discriminant Δ_δ can be used in an experiment where one is comparing the measured $\nu_e \to \nu_\mu$ oscillation probability as a function of the neutrino energy E_ν compared to a "Monte-Carlo prediction" of the spectrum in absence of δ-phase.

2. $\Delta_{CP}(\delta) \equiv P(\nu_e \to \nu_\mu, \delta) - P(\bar{\nu}_e \to \bar{\nu}_\mu, \delta)$
   The discriminant Δ_{CP} can be used in an experiment by comparing the appearance of ν_μ (resp. $\bar{\nu}_\mu$) in a beam of stored μ^+ (resp. μ^-) decays as a function of the neutrino energy E_ν.

3. $\Delta_T(\delta) \equiv P(\nu_e \to \nu_\mu, \delta) - P(\nu_\mu \to \nu_e, \delta)$ or $\bar{\Delta}_T(\delta) \equiv P(\bar{\nu}_e \to \bar{\nu}_\mu, \delta) - P(\bar{\nu}_\mu \to \bar{\nu}_e, \delta)$
   The discriminant Δ_T can be used in an experiment by comparing the appearance of ν_μ (resp. $\bar{\nu}_\mu$) **and** $\bar{\nu}_e$ (resp. ν_e) and in a beam of stored μ^+ (resp. μ^-) decays as a function of the neutrino energy E_ν.

Each of these discriminants have their advantages and disadvantages.

The $\Delta\delta$-method consists in searching for distortions in the visible energy spectrum of events produced by the δ-phase. While this method can in principle provide excellent determination of the phase limited only by the statistics of accumulated events, in practice, systematic effects will have to be carefully kept under control in order to look for a small effect in a seen-data versus Monte-Carlo-expected comparison. In addition, the precise knowledge of the other oscillation parameters will be important, and as will be discussed below, there is a risk of degeneracy between solutions and a possible strong correlation with the θ_{13} angle at high energy.

The Δ_{CP} is quite straight-forward, since it involves comparing the appearance of so-called wrong-sign muons for two polarities of the stored muon beam. It really takes advantage from the fact that experimentally energetic muons are rather easy to detect and identify due to their penetrating nature, and with the help of a magnetic field, their charge can be easily measured, in order to suppress the non-oscillated background from the beam. A non-vanishing Δ_{CP} should in principle be a direct proof for a non-vanishing δ-phase. This method suffers, however, from the inability to perform long-baseline experiment through vacuum. Indeed, matter effects will largely "spoil" Δ_{CP} since it involves both neutrinos and antineutrinos, which will oscillate very differently through matter. Hence, the Δ_{CP} requires a good understanding of the effects related to matter. In addition, it involves measuring neutrinos and antineutrinos. The matter suppression of the antineutrinos will in practice determine the statistical accuracy with which the discriminant can be measured.

Finally, the Δ_T is the theoretically cleanest method, since it does not suffer from the problems of $\Delta\delta$ and Δ_{CP}. Indeed, a difference in oscillation probabilities between $\nu_e \to \nu_\mu$ and $\nu_\mu \to \nu_e$ would be a direct proof for a non-vanishing δ-phase. In addition, matter affects both probabilities in a same way, since it involves only neutrinos. Unfortunately, it is experimentally very challenging to discriminate the electron charge produced in the events, needed in order to suppress the background from the beam. However, one can decide to measure only neutrinos, which are enhanced by matter effects, as opposed to antineutrinos in the Δ_{CP} which were matter suppressed, and hence the statistical accuracy of the measurement will be determined by the efficiency to recognize the electron charge, rather than by matter suppression.

6.1 The L/E_ν scaling

Regardless of their advantages and disadvantages, there is one thing in common between the three discriminants Δ_δ, Δ_{CP} and Δ_T: their behavior with respect to the neutrino energy E_ν and the baseline L. By explicit calculation, we find

$$\begin{aligned}\Delta_\delta &= -\frac{1}{2}c_{13}^2 \sin 2\theta_{12} s_{13} \sin 2\theta_{23} \times \\ &\quad \Big[\cos 2\Delta_{13} - \cos 2\Delta_{23} - 2\cos 2\theta_{12}\sin^2\Delta_{12} + \sin 2\Delta_{12} - \sin 2\Delta_{13} + \sin 2\Delta_{23}\Big] \\ &= -\frac{1}{2}c_{13}^2 s_{13}\Big[\cos 2\Delta_{13} - \cos 2\Delta_{23} + \sin 2\Delta_{12} - \sin 2\Delta_{13} + \sin 2\Delta_{23}\Big]\end{aligned} \tag{41}$$

where for the second line we assumed for simplicity $\theta_{12} = \theta_{23} = \pi/4$, and similarly,

$$\begin{aligned}\Delta_{CP} = \Delta_T &= c_{13}^2 s_{13} \sin 2\theta_{12} \sin 2\theta_{23} \sin\delta\Big[\sin 2\Delta_{12} - \sin 2\Delta_{13} + \sin 2\Delta_{23}\Big] \\ &= -c_{13}^2 s_{13} \sin 2\theta_{12} \sin 2\theta_{23} \sin\delta\Big[\sin\Delta_{12}\sin\Delta_{13}\sin\Delta_{23}\Big]\end{aligned} \tag{42}$$

As expected, both expressions vanish in the limit $\Delta m_{12}^2 \to 0$ where $\Delta m_{13}^2 \to \Delta m_{23}^2$. Also, as one reaches the higher energies, the terms $\Delta_{CP} = \Delta_T$ vanish as

$$\begin{aligned}|\Delta_{CP}| = |\Delta_T| &\simeq c_{13}^2 s_{13} \sin 2\theta_{12} \sin 2\theta_{23} \sin\delta \Delta m_{12}^2 \left(\frac{L}{4E_\nu}\right) \sin^2\left(\Delta m_{23}^2 \frac{L}{4E_\nu}\right) \\ &\simeq c_{13}^2 s_{13} \sin 2\theta_{12} \sin 2\theta_{23} \sin\delta \Delta m_{12}^2 (\Delta m_{23}^2)^2 \left(\frac{L}{4E_\nu}\right)^3\end{aligned} \tag{43}$$

hence, in the very high energy limit at fixed baseline, the effects decrease as E_ν^{-3}. That the effects disappear at high energy is expected, since in this regime, the "oscillations" of the various Δ_{jk}'s wash out.

At high energy, we can also approximate $\cos 2\Delta_{13} \approx \cos 2\Delta_{23} \approx 1$, and find

$$|\Delta_\delta| \simeq \frac{1}{2}\Delta_{CP}(\delta = \pi/2) = \frac{1}{2}\Delta_T(\delta = \pi/2) \tag{44}$$

so the CP- or T-conjugation is equivalent to a change of phase $\delta \to -\delta$, i.e. $\delta = +\pi/2 \to \delta = -\pi/2$.

The important point is that all expressions depend upon some factors which contain the various mixing angles, multiplied by oscillatory terms which always vary like sine or cosine of Δ_{jk}-terms (the terms in squared brackets in the expressions above).

Hence, we expect the various discriminants to scale like $\Delta_{jk} \propto L/E_\nu$. The sensitivity to the δ-phase will therefore follow the behavior of the oscillation probability, and we therefore argue that the maximum of the effect will occur around the "first maximum" of the oscillations, i.e. for $E_\nu^{max} \equiv \Delta m^2_{32} L/2\pi$ (see Eq. (16)).

Strictly speaking, the maximum of the δ-phase sensitivity does not lie exactly at the "first maximum" as defined in Eq. (16). From Eq. (42), we expect the maximum to be "shifted" to higher values of L/E_ν, since it corresponds to the maximum of the term

$$\sin\Delta_{12}\sin\Delta_{13}\sin\Delta_{23} \simeq \Delta m^2_{12}\frac{L}{4E_\nu}\sin^2\left(\Delta m^2_{23}\frac{L}{4E_\nu}\right) \tag{45}$$

which has the functional form $x\sin^2 x$ and, therefore, has its maximum shifted to higher values of x compared to $\sin^2 x$. This small shift is smaller than the oscillation wavelength itself, and does not cause a major problem, since experimentally we will always have sufficient energy range to cover the full oscillation.

These considerations are strictly true only for propagation in vacuum. When neutrinos propagate through matter, matter effects will alter these conclusions. We will however show that as long as the baseline is smaller than some distance such that the corresponding "first maximum" E_ν^{max} lies below the MSW resonance neutrino energy E_ν^{res}, the considerations related to the L/E_ν scaling are still largely valid.

To illustrate this, we show in Figure 9 the rescaled probability for $\nu_e \to \nu_\mu$ oscillations involving neutrinos and as a function of L/E_ν, for three baselines $L = 730$ km, 2900 km, 7400 km and in vacuum (independent of baseline). We assume $\delta = 0$. We readily observe that for the shortest baseline $L = 730$ km the curve is very similar to the one in vacuum. For the middle baseline $L = 2900$ km, the curve is modified with respect to the vacuum case, in the sense that the probability around $(L/E_\nu)^{max} \simeq 400$ (see Eq.17) is enhanced, but for $(L/E_\nu) \lesssim 130$ the probability is smaller than that in vacuum. For the longest baseline $L = 7400$ km, the curve is highly distorted by matter and already for $(L/E_\nu) \lesssim 400$ is the probability smaller than that in vacuum.

In what way does the matter effect alter the ability to look for effects related to the δ-phase? It is incorrect to believe that only the Δ_{CP} discriminant will be affected by propagation through matter, since it is the only one to a priori mix neutrinos and antineutrinos. In reality, the "dangerous" effect of matter is to reduce the dependence of the probability on the δ-phase, and this for any kind of discriminant.

In matter, we would for example write the Δ_T discriminant as

$$|\Delta_T^m| \;=\; (c_{13}^m)^2 s_{13}^m \sin 2\theta_{12}^m \sin 2\theta_{23}^m \sin\delta^m \Big[\sin\Delta_{12}^m \sin\Delta_{13}^m \sin\Delta_{23}^m\Big]$$

$$\simeq \quad (c_{13}^m)^2 s_{13}^m \sin 2\theta_{12}^m \sin 2\theta_{23} \sin\delta \Big[\sin\Delta_{12}^m \sin\Delta_{13}^m \sin\Delta_{23}^m\Big] \tag{46}$$

where because of our choice of Δm^2_{jk}'s, we have $\theta_{23}^m \approx \theta_{23}$ and $\delta^m \approx \delta$ (see Eq. (34)). This implies that the δ-phase discriminants have a different structure that the terms that define the probability of the oscillation (i.e. the non δ-phase dependent terms). The discriminants are the products of sines and cosines of *all* mixing angles and of the Δ_{jk}'s (see Eqs. (41) and (42)). Because of this structure, their property in matter is different.

The Jarlskog's determinant can be shown to be "invariant" under matter effects[25] in the sense that the product

$$J\Big(\Delta m^2_{12}\Delta m^2_{13}\Delta m^2_{23}\Big) \equiv c_{13}^2 s_{13} \sin 2\theta_{12} \sin 2\theta_{23} \sin\delta \Big(\Delta m^2_{12}\Delta m^2_{13}\Delta m^2_{23}\Big) \tag{47}$$

is *independent* from matter effects. This point was also discussed in Ref.[16], where it was pointed out that this implies that the δ-phase terms will be independent from the matter effects as long as we can approximate

$$\sin\Delta_{12} \sin\Delta_{13} \sin\Delta_{23} \approx \Delta_{12}\Delta_{13}\Delta_{23}. \tag{48}$$

This fact is not very revelant in the current context, since the best sensitivity to the δ-phase is expected just when this approximation is *not* valid (i.e. $|\Delta_{13}| \approx |\Delta_{23}| \approx 1$), otherwise the effects wash out. As a consequence, we expect that the CP-odd terms *do* depend on matter effects in the relevant baseline and energy region.

The behavior for neutrino energies above the MSW resonance E_ν^{res} is determined by the fact that in this energy regime, $\theta_{13}^m(E > E_\nu^{res}) \to \pi/2$ and therefore $c_{13}^m \to 0$ and $s_{13}^m \to 1$. More explicitly, one can show that

$$\begin{aligned}
(c_{13}^m)^2 s_{13}^m &\propto E_\nu^{-2} \\
\sin 2\theta_{23}^m &\simeq \sin 2\theta_{23} = const. \\
\sin 2\theta_{12}^m &\to const. \\
\Delta M^2_{31} &\approx \Delta M^2_{32} \propto E_\nu \\
\Delta M^2_{21} &\approx \Delta m^2_{32} = const
\end{aligned} \tag{49}$$

Therefore,

$$|\Delta_T^m| \quad \propto \quad E_\nu^{-2} \sin\delta \Big[\sin\left(\Delta m^2_{32}\frac{L}{4E_\nu}\right) \sin^2\left(\Delta M^2_{13}\frac{L}{4E_\nu}\right)\Big] \propto E_\nu^{-3} \tag{50}$$

and one recovers a neutrino energy dependence identical to that in vacuum (see Eq. (43)). Note also that the argument of the sine function $\Delta M^2_{13} L/4E_\nu$ is *not* small (i.e. the approximation $\sin x \simeq x$ is not valid). For our choice of oscillation parameters, the mass difference is approximately equal to $\Delta M^2_{13}(\mathrm{eV}^2) \simeq 3 \times 10^{-4} \times \mathrm{E}_\nu(\mathrm{GeV})$, and hence the dependence on the baseline is

$$|\Delta_T^m| \quad \propto \quad E_\nu^{-2} \sin\delta \Big[\sin\left(1.27\Delta m^2_{32}\frac{L(\mathrm{km})}{E_\nu(\mathrm{GeV})}\right) \sin^2\left(3.8 \times 10^{-4} L(\mathrm{km})\right)\Big] \tag{51}$$

Hence, the discriminant will first be enhanced and then be suppressed by matter effects. The maximum is found when the sine squared function reaches a maximum, or at approximately 4000 km under the assumption of high energy neutrinos. We will verify numerically that this is really the case in Section 8.

As anticipated, these discussions say that if one wants to study oscillations in the region of the "first maximum", one should not choose a too large baseline L, otherwise, matter effects will suppress the oscillation probability. This is even more so true, as it will be recalled below, that the magnitude of the effects related to the δ-phase are suppressed more rapidly than the oscillation.

The simplest way to express the condition on the matter is to require that the energy of the "first maximum" be smaller than the MSW resonance energy:

$$2\sqrt{2}G_F n_e E_\nu^{max} \lesssim \Delta m^2_{32} \cos 2\theta_{13} \tag{52}$$

and, by inserting the definition of $E_\nu^{max} \equiv \Delta m^2_{32} L/2\pi$ we get

$$\begin{aligned} L_{max} &\lesssim \frac{\pi \cos 2\theta_{13}}{\sqrt{2}G_F n_e} \approx \frac{\pi \cos 2\theta_{13}}{2 \times 1.27 \times 7.56 \times 10^{-5} (\mathrm{eV}^2) \rho(\mathrm{g/cm}^3)} \\ &\approx \frac{1.5 \times 10^4 (\mathrm{km})}{\rho(\mathrm{g/cm}^3)} \approx 5000 \text{ km} \end{aligned} \tag{53}$$

To summarize, we find that *the discriminants of the δ-phase all scale with L/E_ν. The most favorable choice of neutrino energy E_ν and baseline L is in the region of the "first maximum" given by $(L/E_\nu)^{max} \simeq 400$ for $|\Delta m^2_{32}| = 3 \times 10^{-3}$ eV^2.* This leaves a great flexibility in the choice of the actual neutrino energy and the baseline, since only their ratio L/E_ν is determinant. Because of the rising neutrino cross-section with energy, we will see below that it will more favorable to go to higher energies if the neutrino fluency is constant.*Keeping the L/E_ν ratio constant, this implies an optimization at longer baselines L. One will hence gain with the baseline L until we reach $L_{max} \approx 5000$ km beyond which matter effects will spoil our sensitivity.*

7 Detection of Δ_δ at the NF

We begin the discussion with the detection of the δ-phase with the method of the Δ_δ discriminant. We recall that this method implies the comparison of the measured $\nu_e \to \nu_\mu$ oscillation probability as a function of the neutrino energy E_ν compared to a "Monte-Carlo prediction" of the spectrum in absence of δ-phase.

We first illustrate that the discriminant really scales like L/E_ν in Figure 10, where the rescaled Δ_δ discriminant is shown as a function of the L/E_ν ratio. The plot is computed for neutrinos propagating in matter at three different baselines $L = 730$ km, 2900 km and 7400 km, and for neutrinos propagating in vacuum. Indeed, for the

shortest two baselines $L = 730$ km and 2900 km, the value of the discriminant is very similar to that obtained in vacuum. For the longest baseline $L = 7400$ km, well above L_{max} (see Eq. (53)), the effect is highly suppressed by matter effect, since the "first maximum" corresponds for the given baseline L to an energy E_ν above the MSW resonance energy E_ν^{res}.

From the figure, we clearly also see that the effect is largest around the "first maximum", in the region given by $(L/E_\nu)^{max} \simeq 400$.

Given the freedom in the energy E_ν and baseline L, provided the ratio L/E_ν is appropriately chosen, and given the matter effects at distances beyond ≈ 5000 km, we restrict our choices to the two baselines $L = 730$ km and 2900 km.

7.1 The correlation with θ_{13}

When searching for effects related to the δ-phase by comparing the measured $\nu_e \to \nu_\mu$ oscillation probability as a function of the neutrino energy E_ν to a "Monte-Carlo prediction" of the spectrum in absence of δ-phase, requires necessarily a precise knowledge of the other oscillation parameters entering in the oscillation probability expression.

In particular, the knowledge of the angle θ_{13} could be quite important. Indeed, the $\nu_e \to \nu_\mu$ oscillation is primarily driven by the θ_{13} angle and only thanks to a different energy dependence of the terms proportional to δ than to those independent of δ can one hope to determine θ_{13} and δ at the same time!

This is however not true at high energy, when both $|\Delta_{12}| \ll 1$ and $|\Delta_{13}|, |\Delta_{23}| \ll 1$. This can be explicitly shown for example for simplicity in the limit of small θ_{13}. The rescaled probability is in this case (see Eq. (26)) a constant:

$$p(\nu_e \to \nu_\mu) \simeq \frac{(\Delta m^2_{12})^2}{32}\Big\{1 + 2Ms^2_{13} + 8Ns_{13}\cos\delta\Big\} \tag{54}$$

where $M = ((\Delta m^2_{13})^2 + (\Delta m^2_{23})^2)/(\Delta m^2_{12})^2$ and $N = (\Delta m^2_{13} + \Delta m^2_{23})/(\Delta m^2_{12})$. The absence of "oscillations" at high energy implies that a change of θ_{13} can mimic a change of δ.

To illustrate this effect in a concrete example, we show in Figures 11 and 12 the rescaled probabilities for the two baselines $L = 730$ km and 2900 km as a function of neutrino energy E_ν. The probabilities are computed for neutrinos in matter (full line) and in vacuum (dotted line), and for three values of the δ-phase: $\delta = 0$, $\delta = +\pi/2$, $\delta = -\pi/2$.

At the shortest baseline $L = 730$ km, this behavior can be clearly seen for $E_\nu \gtrsim 20$ GeV. The two curves for $\delta = +\pi/2$ and $\delta = -\pi/2$ tend to a constant, which is clearly different than the constant for $\delta = 0$, but that cannot be distinguished from a $\delta = 0$ with a different θ_{13}. In addition, we recall that the reason that both $\delta = +\pi/2$ and $\delta = -\pi/2$ tend to the same constant, is due to the fact that the probability at high energy depends only on $\cos\delta$ (see Eq. (26)).

At the longer baseline $L = 2900$ km, the situation is improved since up to $\approx$ 100 GeV, the rescaled probability is clearly not a constant, but rather still falling with energy. We also point out that one can visually see that most of the sensitivity at $L = 2900$ km is for neutrino energies around 10 GeV or so. This is an important point to take into account when considering the muon detection threshold of a given experimental setup.

8 Direct detection of T-violation at the NF

We now turn to the most challenging search for effects related to δ and consider the Δ_T discriminant. We recall here that the discriminant Δ_T implies the comparison between the appearance of ν_μ (resp. $\bar{\nu}_\mu$) **and** $\bar{\nu}_e$ (resp. ν_e) in a beam of stored μ^+ (resp. μ^-) decays as a function of the neutrino energy E_ν.

The Δ_T method takes in advantage that deals with differences between neutrinos (or anti-neutrinos) only, so matter effects give only a scale factor and no "CP-fake" violation effects are expected for δ=0. So, the comparison of $\nu_\mu \to \nu_e$ and $\nu_e \to \nu_\mu$ oscillation probabilities offers a direct way to highlight a complex component in the mixing matrix, independent of matter and other oscillation parameters.

This is clearly visible in Figure 13, where the rescaled value of Δ_T is shown for three baselines and for vacuum. The magnitude of the T-violation effect is roughly the same for vacuum, 730 km and 2900 km, while for very long baselines (7400 km) the sensitivity is lost. As described in Section 6.1, all δ-phase discriminants scale with L/E_ν until L$\approx$5000 km (see equation 53) and because of matter effects, beyond this value the effect decreases dramatically.

The drop of the rescaled Δ_T for very long baselines is also illustrated in Figure 14. The rescaled Δ_T discriminant is shown as a function of the baseline and of the neutrino energy, for neutrinos in vacuum (top) and in matter (bottom) for $\delta = +\pi/2$. In vacuum, the same value of $\Delta_T \times E^2/L^2$ is obtained keeping the L/E_ν ratio constant, while in matter this pattern is destroyed, loosing in sensitivity for long baselines. For instance, for $E_\nu \sim 12$ GeV, the discriminant starts dropping for baselines larger than 4000 km.

As already pointed out, the major difficulty of the Δ_T method is that it requires the measurement of the electron charge in order to discriminate the large ν_e background from the beam. Both, the wrong-sign muon and the wrong-sign electron samples are needed to build the magnitude.

9 Direct detection of CP-violation at the NF

We now continue our discussion and consider the Δ_{CP} discriminant. We recall that the Δ_{CP} is in principle quite straight-forward, since it involves comparing the appearance

of ν_μ (resp. $\bar{\nu}_\mu$) in a beam of stored μ^+ (resp. μ^-) decays as a function of the neutrino energy E_ν. A non-vanishing Δ_{CP} obtained from an observation of the two polarities of the stored muon beam would be a direct proof for a non-vanishing δ-phase.

However, as already pointed out, this method suffers from the practical necessity to traverse the Earth matter in order to perform long baseline experiments.

Since neutrinos and anti-neutrinos are affected by matter with an "opposite sign", the matter terms will not cancel in the Δ_{CP} discriminant. As a result, the Δ_{CP} will not necessarily vanish when $\delta = 0$ (having the so called "CP-fake" violation effects. Hence, a direct detection of a non-vanishing Δ_{CP} discriminant does not imply $\delta \neq 0$.

We illustrate this situation in Figure 15, where the rescaled Δ_{CP} discriminant is plotted as a function of the neutrino energy E_ν, computed for neutrinos propagating in matter at three different baselines $L = 730$ km, 2900 km and 7400 km. Three sets of curves are represented, corresponding to $\delta = +\pi/2$, $\delta = -\pi/2$ and $\delta = 0$.

At the shortest baseline $L = 730$ km, we observe that the maximum of the effect is indeed around the "first maximum" at about a neutrino energy of 2 GeV. For $\delta = 0$ (thin curve), the discriminant does not vanish, due to matter. This effect is however smaller than the "genuine" effect at $|\delta| = \pi/2$ and we observe that for $\delta = +\pi/2 \longrightarrow -\pi/2$ the discriminant changes sign.

For the medium baseline of $L = 2900$ km, the maximum of the effect is again near the "first maximum" ($E_\nu \equiv 8$ GeV). The $\Delta_{CP} \times E^2/L^2$ discriminant is larger (a factor 2) than for $L = 730$ km in the case of $\delta = +\pi/2$, but this includes the "CP-fake" contribution coming from matter. In order to compare at both baselines the "genuine" CP-violation effect (the one due to a non zero δ-phase) one has to compute the difference between $\delta = +\pi/2$ and $\delta = -\pi/2$, resulting similar at both baselines. Another interesting feature is that, at $L = 2900$ km the discriminant is already positive for any value of δ.

At larger baselines ($L = 7400$ km) Δ_{CP} is completely dominated by matter effects. The three values of δ mix and the sensitivity on Δ_{CP} to the "genuine" CP-violation is lost.

Finally, we address the scaling of the effect with L/E_ν. Figure 16 shows the same set of curve displayed in Figure 15, but as a function of the L/E_ν ratio. In addition to the three different baselines, the case of neutrinos propagating in vacuum (independent of baseline) is also shown for comparison. At 730 km and 2900 km the effect is maximum for the same $L/E_\nu \simeq 400$ km/GeV (for $\Delta m^2_{32} = 3 \times 10^{-3}$ eV^2). In addition, the difference between $\delta = +\pi/2$ and $-\pi/2$ at the maximum is similar for both baselines.

10 Behavior for small θ_{13} values

In the above sections, the possibility of detecting CP-violation, based on the comparison of oscillations involving electron and muon (anti-)neutrinos has been discussed. This transition is strongly dependent on the value of the mixing angle θ_{13}, and it is natural to ask how the sensitivity to CP-violation varies with the value of this angle. It was stated ([26]) that, "as far as the Δm^2_{21} effects in the CP-conserving part of the oscillation probability can be neglected", the sensitivity to CP-violation does not depend on θ_{13}.

We can check this hypothesis directly with the help of our Eq. 11. The probability for oscillations depends on

$$\begin{aligned} & 4\underline{c^2_{13}}\Big[\sin^2\Delta_{23}s^2_{12}\underline{s^2_{13}}s^2_{23}+c^2_{12}\left(\sin^2\Delta_{13}\underline{s^2_{13}}s^2_{23}+\sin^2\Delta_{12}s^2_{12}\left(1-\left(1+\underline{s^2_{13}}\right)s^2_{23}\right)\right)\Big] \\ \approx\ & 4\Big[\sin^2\Delta_{23}s^2_{12}\underline{s^2_{13}}s^2_{23}+c^2_{12}\left(\sin^2\Delta_{13}\underline{s^2_{13}}s^2_{23}\right)\Big] \end{aligned} \tag{55}$$

where we have neglected Δ_{12}. The parts dependent on δ go like

$$\begin{aligned} -\frac{1}{2}c^2_{13}\sin(2\theta_{12})\underline{s_{13}}\sin(2\theta_{23})\cos\delta\left[\cos 2\Delta_{13}-\cos 2\Delta_{23}-2\cos(2\theta_{12})\sin^2\Delta_{12}\right] \\ +\frac{1}{2}c^2_{13}\ \sin\delta\sin(2\theta_{12})\underline{s_{13}}\sin(2\theta_{23})\left[\sin 2\Delta_{12}-\sin 2\Delta_{13}+\sin 2\Delta_{23}\right] \end{aligned} \tag{56}$$

As can be seen, the δ-dependent part of the probability depends on $\sin\theta_{13}$, while the leading term (and the total number of oscillated events) is proportional to $\sin^2\theta_{13}$.

In the Gaussian approximation, the statistical error is proportional to the square root of the number of events, so the significance of the δ-effects is independent of θ_{13}. The validity of this assumption will depend on the total number of muon decays and on the total mass of the considered detector.

As far as the Δm^2_{21} part is concerned, the approximation is valid if

$$\sin^2\Delta_{13}\underline{s^2_{13}}s^2_{23}\gtrsim\sin^2\Delta_{12}s^2_{12}\left(1-\left(1+\underline{s^2_{13}}\right)s^2_{23}\right) \tag{57}$$

or

$$s_{13}\gtrsim\sqrt{\frac{\sin^2\Delta_{12}}{2\sin^2\Delta_{13}}}\approx 0.02\frac{\Delta m^2_{12}}{10^{-4}(\mathrm{eV}^2)} \tag{58}$$

and $\Delta m^2_{23}=3\times10^{-3}eV^2$. For smaller values of θ_{13}, the oscillation probability is dominated by the constant term, and the cancellation of the θ_{13} dependence no longer applies.

11 Two concrete cases at 730 and 2900 km

In order to assess with concrete examples the use of the δ-phase discriminants, we consider the two baselines, with corresponding muon beam energy and matter densities:

Baseline	E_μ	Muon decays	Matter density
732 km	7.5 GeV	10^{21}	2.8 g/cm^3
2900 km	30 GeV	2.5×10^{20}	3.2 g/cm^3

Both examples were chosen to have the same L/E_μ and include matter effects. Because of the linear rise of the neutrino cross-section with E_ν, the factor 4 in muon energy between the 732 km and 2900 km case, is "compensated" by an increase of intensity by the same factor in favor of the shorter baseline.

We compute the fluxes assuming unpolarized muons and disregarding muon beams divergences within the storage ring. We consider that 50% of the stored muons decay on the direction of the detector ("useful" muons). We integrate the expected event rates using a neutrino-nucleon Monte-Carlo generator[27]. The total charged current (CC) cross section is technically subdivided into three parts: the exclusive quasi-elastic scattering channel σ_{QE} and the inelastic cross section $\sigma_{inelasic}$ which includes all other processes except charm production which is included separately. Event rates for the two energy-baseline-flux combinations are shown in Tables 1 and 2 for a 10 kton fiducial mass detector.

Our analyses are performed on samples of fully generated Monte-Carlo events[27], which include proper kinematics of the events, full hadronization of the recoiling jet and proper exclusive polarized tau decays when relevant. Nuclear effects, which are taken into account by the FLUKA model, are included as they are important for a proper estimation of the tau kinematical identification.

To have a proper account for the detector and background effects, the specific detector model of a Liquid Argon TPC[6] has been assumed.

The detector response is included in our analyses using a fast simulation which parameterizes the momentum and angular resolution of the emerging particles, using essentially the following values: electromagnetic shower $3\%/\sqrt{E} \oplus 1\%$, hadronic shower $\approx 20\%/\sqrt{E} \oplus 5\%$, and magnetic muon momentum measurement 20%.

11.1 Lepton charge identification

Muon identification, charge and momentum measurement provide discrimination between ν_μ and $\bar{\nu}_\mu$ charged current (CC) events. Good ν_e CC versus ν NC discrimination relies on the fine granularity of the target. Finally, the identification of ν_τ CC events requires a precise measurement of all final state particles.

	Process	$E_\mu = 7.5$ GeV $L = 732$ km 10^{21} μ^-	$E_\mu = 30$ GeV $L = 2900$ km 2.5×10^{20} μ^-
Non-oscillated rates	ν_μ CC	39572	35945
	ν_μ NC	10775	10688
	$\bar{\nu}_e$ CC	14419	13911
	$\bar{\nu}_e$ NC	4501	4830
Oscillated events ($\delta = \pi/2$)	$\bar{\nu}_e \rightsquigarrow \bar{\nu}_\mu$ CC	85	42
	$\nu_\mu \rightsquigarrow \nu_e$ CC	248	238
Oscillated events ($\delta = 0$)	$\bar{\nu}_e \rightsquigarrow \bar{\nu}_\mu$ CC	134	72
	$\nu_\mu \rightsquigarrow \nu_e$ CC	370	333
Oscillated events ($\delta = -\pi/2$)	$\bar{\nu}_e \rightsquigarrow \bar{\nu}_\mu$ CC	134	69
	$\nu_\mu \rightsquigarrow \nu_e$ CC	360	323

Table 1: Event rates for a 10 kton detector. The oscillation parameters are: $\Delta m^2_{32} = 3 \times 10^{-3}$ eV^2, $\Delta m^2_{12} = 1 \times 10^{-4}$ eV^2, $\sin^2\theta_{23} = 0.5$, $\sin^2\theta_{12} = 0.5$ and $\sin^2 2\theta_{13} = 0.05$.

	Process	$E_\mu = 7.5$ GeV $L = 732$ km 10^{21} μ^+	$E_\mu = 30$ GeV $L = 2900$ km 2.5×10^{20} μ^+
Non-oscillated rates	$\bar{\nu}_\mu$ CC	16472	16054
	$\bar{\nu}_\mu$ NC	5319	5636
	ν_e CC	35279	31399
	ν_e NC	9268	9245
Oscillated events ($\delta = \pi/2$)	$\nu_e \rightsquigarrow \nu_\mu$ CC	408	389
	$\bar{\nu}_\mu \rightsquigarrow \bar{\nu}_e$ CC	123	66
Oscillated events ($\delta = 0$)	$\nu_e \rightsquigarrow \nu_\mu$ CC	403	381
	$\bar{\nu}_\mu \rightsquigarrow \bar{\nu}_e$ CC	128	71
Oscillated events ($\delta = -\pi/2$)	$\nu_e \rightsquigarrow \nu_\mu$ CC	266	273
	$\bar{\nu}_\mu \rightsquigarrow \bar{\nu}_e$ CC	84	43

Table 2: Same as Table 1, but μ^+ decays.

$\mu^- \rightarrow e^- \nu_\mu \bar{\nu}_e$

Right sign muons (μ^-):			
	ν_μ	CC	
	$\nu_\mu \rightsquigarrow \nu_\tau$	CC	$(\tau^- \rightarrow \mu^-)$
	$\bar{\nu}_e$	NC	$(\pi^- \rightarrow \mu^-)$
	ν_μ	NC	$(\pi^- \rightarrow \mu^-)$
Wrong sign muons (μ^+):			
	$\bar{\nu}_e \rightsquigarrow \bar{\nu}_\mu$	CC	
	$\bar{\nu}_e \rightsquigarrow \bar{\nu}_\tau$	CC	$(\tau^+ \rightarrow \mu^+)$
	$\bar{\nu}_e$	NC	$(\pi^+ \rightarrow \mu^+)$
	ν_μ	NC	$(\pi^+ \rightarrow \mu^+)$
Electrons:			
	$\bar{\nu}_e$	CC	$(\bar{\nu}_e \rightarrow e^+)$
	$\nu_\mu \rightsquigarrow \nu_e$	CC	$(\nu_e \rightarrow e^-)$
	$\nu_\mu \rightsquigarrow \nu_\tau$	CC	$(\tau^- \rightarrow e^-)$
	$\bar{\nu}_e \rightsquigarrow \bar{\nu}_\tau$	CC	$(\tau^+ \rightarrow e^+)$
Wrong sign electrons (e^-):			
	$\bar{\nu}_e$	CC	$(\bar{\nu}_e \rightarrow e^+) \times p_{conf}$
	$\nu_\mu \rightsquigarrow \nu_e$	CC	$(\nu_e \rightarrow e^-) \times (1 - p_{conf})$
	$\nu_\mu \rightsquigarrow \nu_\tau$	CC	$(\tau^- \rightarrow e^-) \times (1 - p_{conf})$
	$\bar{\nu}_e \rightsquigarrow \bar{\nu}_\tau$	CC	$(\tau^+ \rightarrow e^+) \times p_{conf}$
Neutral Currents (no leptons):			
	ν_μ	NC	(hadrons)
	$\nu_\mu \rightsquigarrow \nu_\tau$	CC	$(\tau^- \rightarrow$ hadrons$)$
	$\bar{\nu}_e$	NC	(hadrons)
	$\bar{\nu}_e \rightsquigarrow \bar{\nu}_\tau$	CC	$(\tau^+ \rightarrow$ hadrons$)$

Table 3: Event classes in case of μ^- beam.

It is natural to classify the events in various classes depending on their final state configuration[28]. We illustrate them for the case of μ^- stored in the ring.

1. **Right sign muons ($rs\mu$):** the leading muon has *the same charge* as those circulating inside the ring. We include the non-oscillated ν_μ CC events, the $\nu_\mu \rightarrow \nu_\tau$ oscillations charged current events followed by $\tau \rightarrow \mu$ and the background from hadron decays in neutral currents induced by all neutrino flavors.

2. **Wrong sign muons ($ws\mu$):** the leading muon has *opposite charge* to those circulating inside the ring. Opposite-sign leading muons can only be produced by neutrino oscillations, since there is no component in the beam that could account for them. This includes $\bar{\nu}_e \rightarrow \bar{\nu}_\mu$ oscillations and $\bar{\nu}_e \rightarrow \bar{\nu}_\tau$ oscillations

with $\tau^+ \to \mu^+$ decays. We also include hadron decays in neutral currents induced by all neutrino flavors.

3. **Electrons (e):** events with a prompt electron (*both charges*) and no primary muon identified. Events with leading electron or positron are produced by the charged-current interactions of the following neutrinos: non-oscillated $\bar{\nu}_e$ neutrinos, $\nu_\mu \to \nu_e$ oscillations and $\bar{\nu}_e \to \bar{\nu}_\tau$ or $\nu_\mu \to \nu_\tau$ oscillations with $\tau \to e$ decays

4. **Wrong sign electrons (wse):** the leading electron has an identified charge which has *the same sign* as that of the muons circulating inside the ring. We define

   - the efficiency ϵ_e to identify the charge;
   - the probability p_{conf} for charge confusion.

   Hence, the wrong sign electron sample is built from unoscillated $\bar{\nu}_e$'s from the beam with a weight $P(\bar{\nu}_e \to \bar{\nu}_e) \times \epsilon_e \times p_{conf}$ and from muon neutrinos oscillations with the weight $P(\nu_\mu \to \nu_e) \times \epsilon_e \times (1 - p_{conf})$.

5. **No Lepton (0ℓ):** events corresponding to NC interactions or ν_τ CC events followed by a hadronic decay of the tau lepton. Events with *no leading electrons or muons* will be used to study the $\nu_\mu \to \nu_\tau$ oscillations. These events can be produced in neutral current processes or in $\bar{\nu}_e \to \bar{\nu}_\tau$ or $\nu_\mu \to \nu_\tau$ oscillations with $\tau \to hadrons$ decays.

Table 3 summarizes the different processes that contribute to the five event classes. p_{conf} is the electron charge confusion probability.

For electron or muon charged current events, the visible event energy reconstructs the incoming neutrino energy and is therefore a very important variable to study the energy dependence of the oscillations.

The last three classes can only be cleanly studied in a fine granularity detector.

The energy loss of a minimum ionizing particle in liquid Argon is about 200 MeV/m, while the nuclear interaction length is 84 cm. That means that a muon with a momentum of 0.5 GeV will travel about 2.5 meters before being absorbed, corresponding to about 3 nuclear interaction lengths. The probability that a pion will travel so long without interacting is small, and also detailed simulations show that at this level of background rejection pions do not represent a problem.

Based on preliminary estimates[29], we assume that for electrons with energy less than 7.5 GeV, the charge identification efficiency is 20% with a charge confusion probability of 0.1%, unless otherwise noted.

11.2 Direct extraction of the oscillation probabilities

From the visible energy distributions of the events, one can extract the oscillation probabilities. The visible energy of the events are plotted into histograms with 10 bins in energy. The $\nu_e \to \nu_\mu$ oscillation probability in each energy bin i can be computed as

$$\mathcal{P}_i(\nu_e \to \nu_\mu) = \frac{N_i(ws\mu) - N_i^0(ws\mu)}{\epsilon_i(p_\mu > p_\mu^{cut}) N_i^0(e)} \qquad [\mu^+ \ decays] \tag{59}$$

where $N_i(ws\mu)$ is the number of wrong-sign muon events in the i-th bin of energy, $N_i^0(ws\mu)$ are the background events in the i-th bin of energy, $\epsilon_i(p_\mu > p_\mu^{cut})$ is the efficiency of the muon threshold cut in that bin, and $N_i^0(e)$ is the number of electron events in the i-th bin of energy in absence of oscillations. The number of events corresponds to the statistics obtained from μ^+ decays. A similar quantity for antineutrinos $\mathcal{P}_i(\bar{\nu}_e \to \bar{\nu}_\mu)$ will be computed with events coming from μ^- decays.

Similarly, the $\nu_\mu \to \nu_e$ oscillation probability in each energy bin i can be computed as

$$\mathcal{P}_i(\nu_\mu \to \nu_e) = \frac{N_i(wse) - N_i^0(wse)}{\epsilon_e(1 - p_{conf}) N_i^0(rs\mu)} \qquad [\mu^- \ decays] \tag{60}$$

where $N_i(wse)$ is the number of wrong-sign electron events in the i-th bin of energy, ϵ_e is the efficiency for charge discrimination, p_{conf} the charge confusion, and $N_i^0(rs\mu)$ is the number of right sign muon events in the i-th bin of energy in absence of oscillations. The number of events corresponds to the statistics obtained from μ^- decays. A similar quantity for antineutrinos $\mathcal{P}_i(\bar{\nu}_\mu \to \bar{\nu}_e)$ will be computed with events coming from μ^+ decays.

These binned probabilities could be combined in an actual experiment in order to perform direct searches of the effects induced by the δ-phase.

11.3 Direct search for T-asymmetry

For measurements involving the discrimination of the electron charge, we limit ourselves to the lowest energy and baseline configuration ($E_\mu = 7.5$ GeV and $L = 732$ km), since we expect the discrimination of the electron charge to be practically possible only at these lowest energies.

The binned $\Delta_T(i)$ discriminant for neutrinos is defined as

$$\Delta_T(i) = \mathcal{P}_i(\nu_\mu \to \nu_e) - \mathcal{P}_i(\nu_e \to \nu_\mu) \tag{61}$$

and a similar discrimant $\bar{\Delta}_T(i)$ can be computed for antineutrinos.

These quantities are plotted for neutrinos and antineutrinos for three values of the δ-phase ($\delta = +\pi/2$, $\delta = 0$ and $\delta = -\pi/2$) in Figure 18. The errors are statistical and

correspond to a normalization of 10^{21} muon decays and a baseline of $L = 732$ km. A 20% electron efficiency with a charge confusion probability of 0.1% has been assumed. The full curve corresponds to the theoretical probability difference.

A nice feature of these measurements is the change of sign of the effect with respect of the change $\delta \to -\delta$ and also with respect to the substitution of neutrinos by antineutrinos. These changes of sign are clearly visible and would provide a direct, model-independent, proof for T-violation in neutrino oscillations.

In order to cross-check the matter behavior, one can also contemplate the CPT-discriminants defined as

$$\begin{aligned} \Delta_{CPT}(i) &= \mathcal{P}_i(\nu_\mu \to \nu_e) - \mathcal{P}_i(\bar{\nu}_e \to \bar{\nu}_\mu) \\ \bar{\Delta}_{CPT}(i) &= \mathcal{P}_i(\nu_e \to \nu_\mu) - \mathcal{P}_i(\bar{\nu}_\mu \to \bar{\nu}_e) \end{aligned} \tag{62}$$

These quantities are plotted in Figure 19, with the same assumptions as in Figure 18. The full curve corresponds to the theoretical probability difference. As expected, these quantities are *independent from the δ-phase and probe only the matter effects*. The change of sign of the effect with respect to the substitution of neutrinos by antineutrinos is clearly visible.

It should be however noted that in the case of the CPT discriminant, the statistical power is rather low, since this measurement combines the appearance of electrons (driven by the efficiency for detecting the electron charge) and involves antineutrinos, which are suppressed by matter effects. Hence, the statistical power is reduced compared to the T-discriminant.

11.4 Direct search for CP-asymmetry

In the direct search for the CP-asymmetry, we rely only on the appearance of wrong-sign muons. We compare in this case the two energy and baselines options.

The binned $\Delta_{CP}(i)$ discriminant for the shortest baseline $L = 732$ km, $E_\mu = 7.5$ GeV and longest baseline $L = 2900$ km, $E_\mu = 30$ GeV (lower plots) for three values of the δ-phase ($\delta = +\pi/2$, $\delta = 0$ and $\delta = -\pi/2$) are shown in Figure 20. The errors are statistical and correspond to a normalization of $10^{21}(2.5 \times 10^{20})$ for $L = 732(2900)$ km. The full curve corresponds to the theoretical probability difference. The dotted curve is the theoretical curve for $\delta = 0$ and represents the effect of propagation in matter.

As was already pointed out, the Δ_{CP} does not vanish even in the case $\delta = 0$, since matter introduces an asymmetry. At the shortest baseline ($L = 732$ km), these effects are rather small, as illustrated in Figure 11. This has the advantage that the observed asymmetry would be positive for $\delta > 0$, but would still change sign in the case $\delta \approx -\pi/2$. In the fortunate case in which Nature has chosen such a value for the δ-phase, the observation of the negative asymmetry would be a striking sign for CP-violation, since matter could never produce such an effect.

For other values of the δ-phase, the effect is positive. It is also always positive at the largest baseline $L = 2900$ km, since at those distances the effect induced by the δ-phase is smaller than the asymmetry introduced by the matter.

11.5 Comparison of two methods

The binned $\Delta_T(i)$ and $\Delta_{CP}(i)$ discriminant can be used to calculate the χ^2 significance of the effect, given the statistical error on each bin. We compute the following χ^2's:

$$\chi^2_T = \sum_i \frac{\left(\Delta_T(i,\delta) - \Delta_T(i,\delta=0)\right)^2}{\sigma(\Delta_T(i,\delta))^2} + \frac{\left(\bar{\Delta}_T(i,\delta) - \bar{\Delta}_T(i,\delta=0)\right)^2}{\sigma(\bar{\Delta}_T(i,\delta))^2} \tag{63}$$

where $\sigma(\Delta_T(i,\delta))$ is the statistical error in the bin. Since $\Delta_T(\delta)$ and $\bar{\Delta}_T(\delta)$ use independent sets of data, the global χ^2_T can be computed in this way, as linear sum of both contributions.

Similarly, the χ^2 of the CP-asymmetry is

$$\chi^2_{CP} = \sum_i \frac{\left(\Delta_{CP}(i,\delta) - \Delta_{CP}(i,\delta=0)\right)^2}{\sigma(\Delta_{CP}(i,\delta))^2} \tag{64}$$

We study the significance of the effect as a function of the solar mass difference Δm^2_{21}, since the effect associated to the δ-phase will decrease with decreasing Δm^2_{21} values. We consider the range compatible with solar neutrino experiments, $10^{-5} \lesssim \Delta m^2_{21} \lesssim 10^{-4}$ eV^2.

The exclusion regions obtained at the 90%C.L. (defined as $\Delta\chi^2 = +1.96$) in the δ-phase vs Δm^2_{21} plane are shown in Figure 21. The rest of parameters are fixed to the reference values ($\Delta m^2_{32} = 3 \times 10^{-3}$ eV^2, $\Delta m^2_{21} = 1 \times 10^{-4}$ eV^2, $\sin^2\theta_{23} = 0.5$, $\sin^2\theta_{12} = 0.5$, and $\sin^2 2\theta_{13} = 0.05$). An electron charge confusion probability of 0.1% and an electron detection efficiency of 20% has been assumed. The normalizations assumed are 10^{21} and 5×10^{21} muon decays with energy $E_\mu = 7.5$ GeV and a baseline of $L = 732$ km.

The results are very encouraging. With 10^{21} muon decays, the region $\Delta m^2_{21} \gtrsim 4\times10^{-5}$ eV^2 is covered. For 5×10^{21} muons, this region extends down to 2×10^{-5} eV^2. If we consider that the value of Δm^2_{21} is known and that it has a value of $\Delta m^2_{21} = 10^{-4}$ eV^2, one can constrain the values of the δ-phase within the range $|\delta| \lesssim 0.57$ or $|\delta| \gtrsim 2.6$ for 10^{21} muons and $|\delta| \lesssim 0.12$ and $|\delta| \gtrsim 3.0$ for 5×10^{21} muon decays at the 90%C.L.

Figure 22 shows the same exclusion plot but comparing the two considered L/E_ν values. For L = 730 km, the normalizations are 10^{21} and 5×10^{21} muons, while for L = 2900 km the considered fluxes are four times smaller. Contrary to what happens at short baselines, where a nice symmetry between $+\delta$ and $-\delta$ is observed, at L = 2900 km matter effects introduce a clear asymmetry between the two excluded regions.

We conclude that an exhaustive direct, model-independent exploration of the δ-phase, within the full range $10^{-5} \lesssim \Delta m^2_{21} \lesssim 10^{-4}$ eV^2 requires an intensity of 5×10^{21} muon decays of each sign.

As explained in Section 11.2, the value of the $\nu_\mu \to \nu_e$ oscillation probability (and hence the χ^2_T discriminant) depends on both the electron detection efficiency, ϵ_e, and the electron charge confusion, p_{conf} (see equation 60). In Figure 23 we show the iso-curves at 1σ, 2σ and 3σ levels of significance[3] that can be obtained for $\delta = +\pi/2$ and $-\pi/2$. For instance, in the case of (ϵ_e, p_{conf})=(20%,1%) one could exclude both $\delta = \pm\pi/2$ at 2σ level. Looking at the shape of the iso curves we can conclude that, even if the result depends on both parameters, it is much more sensitive to the value of the charge confusion, which should be smaller than $\sim$0.1% for efficiencies of $\sim$20% to have an exclusion power above 3σ.

11.6 Comparison with the fit of the visible energy distributions

The most effective way to fit the oscillation parameters is to study the visible energy distribution of the four classes of events[4], since assuming the unoscillated spectra are known, they contain direct information on the oscillation probabilities.

Of course, for electron or muon charged current events, the visible energy reconstructs the incoming neutrino energy. In the case of neutral currents or the charged current of tau neutrinos, the visible energy is less than the visible energy because of undetected neutrinos in the final state. The information is in this case degraded but can still be used.

In case no CP-violation is observed, the result of the fit in terms of 2-dimensional 90% C.L. contours in the $\Delta m^2_{12} - \delta$ plane is shown in Figure 24. The `Y` axis spans the Δm^2_{12} range allowed by LMA solar neutrinos, and the whole range $-\pi < \delta < \pi$ has been consider. For each pair of values (Δm^2_{12},δ), the fit to the reference distributions[5] was performed fixing all parameters (lower curves) and leaving θ_{13} free (upper curves). The result for the two considered baselines and energies are shown.

As expected, this method is clearly more powerful than the direct search for CP-asymmetry discussed in Section 11.4. The comparison between both results reveals that the non-excluded zones near the extremes ($|\delta| \sim \pi$) in Figure 21 are now covered and can be explored with this second method (Figure 24). However, even if higher exclusive, the fit of the visible energy distributions requires a good knowledge of the oscillation parameters, while the direct search for CP-asymmetry is essentially model

[3]The $n\sigma$ region is reached when $\sqrt{\chi^2_{\Delta T} + \chi^2_{\Delta \bar{T}}} \geq n$.

[4]In this case, we do not use the information coming from the electron charge.

[5]The reference values are $\Delta m^2_{32} = 3 \times 10^{-3}$ eV^2, $\sin^2\theta_{23} = 0.5$, $\sin^2\theta_{12} = 0.5$, $\sin^2 2\theta_{13} = 0.05$ and $\delta = 0$.

independent. Nevertheless, even assuming that the value of θ_{13} is not known precisely (upper curves in Figure 24) the excluded regions extend beyond the limits set by the first method for $|\delta| \sim \pi$.

The result obtained with the full simulation fully supports all the above phenomenological considerations: for baselines such that the maximum of the interesting effect lies well below the MSW resonance, the destructive effect of matter almost does not play any role, and for a given machine power, if L/E_μ is kept constant, the same sensitivity is reached.

12 Summary and Conclusions

In this document, we have discussed general strategies to detect CP-violation effects related to the complex phase δ of the neutrino mixing matrix, in the framework of a neutrino factory. Here is the summary and conclusions:

• In order to directly compare effects at different energies and baselines, we have defined the "rescaled probability": $P(\nu_\alpha \rightsquigarrow \nu_\beta; E_\nu, L) \times \frac{E_\nu^2}{L^2}$. It approximately weighs the probability by the neutrino energy spectrum of the neutrino factory and by the attenuation of the neutrino flux with the distance (Section 4).

• In vacuum, the region of the "first maximum" on the $\nu_\mu \to \nu_e$ oscillation probability yields $E_\nu^{max} \simeq 2$ GeV at 730 km, $\simeq 8$ GeV at 2900 km and $\simeq 20$ GeV at 7400 km for $\Delta m^2_{32} = 3 \times 10^{-3}$ eV^2. For neutrinos propagating through matter, the oscillation probabilities are distorted and the resonant energy is $E_\nu^{res} \simeq 14.1$, 12.3 and 10.7 GeV for $\Delta m^2_{32} = 3 \times 10^{-3}$ eV^2 and ρ equal to 2.7, 3.2 and 3.7 g/cm^3 respectively.

• *The most favorable choice of neutrino energy E_ν and baseline L is in the region of the "first maximum"* given by $(L/E_\nu)^{max} \simeq 400$ km/GeV for $|\Delta m^2_{32}| = 3 \times 10^{-3}$ eV^2. As discussed in Section 6.1, if one wants to study oscillations in this region one has to require that the energy of the "first-maximum" be smaller than the MSW resonance energy: $2\sqrt{2} G_F n_e E_\nu^{max} \lesssim \Delta m^2_{32} \cos 2\theta_{13}$. This fixes a limit on the baseline $L_{max} \approx$5000 km beyond which matter effects spoil the sensitivity.

This implies that we concentrate on medium L/E_ν.

• We have considered three quantities which are good discriminators for a non-vanishing δ-phase (Section 6): Δ_δ, Δ_{CP} and Δ_T.

Δ_δ can provide excellent determination of the phase, limited only by statistics, but needs a precise knowledge of the other oscillation parameters and possible correlations with the θ_{13} at high energy can appear.

Δ_{CP} has the advantage that involves the appearance of wrong-sign muons only, experimentally easy to detect, but the disadvantage of involving both, neutrinos and antineutrinos, which requires a good understanding of the effects related to matter. Matter effects will largely spoil Δ_{CP} at long distances.

Δ_T is not affected by matter effects because it involves only neutrinos, but it requires to discriminate the electron charge, which is experimentally very challenging. A non-vanishing Δ_T would be a direct proof for a non-vanishing δ-phase.

We have demonstrated that the discriminants of the δ-phase in vacuum scale with L/E_ν (in matter, this scaling remains valid for L smaller than $\sim$5000 km).

• In one hand, because of the linear rise of the neutrino cross-section with neutrino energy at high energy, the statistical significance of the effect scales with E_ν, so it grows linearly with L (for L/E_ν constant).

On the other, the study of Δ_T requires the electron charge identification. *For a constant (L/E_ν) ratio, the need of low energy electrons points towards lower-energy beams and shorter distances.*

• As an example, we have considered two concrete cases keeping the same L/E_μ ratio: (L = 730 km, E_μ = 7.5 GeV) and (L = 2900 km, E_μ = 30 GeV). We have classified the events in five classes (right and wrong sign muons, right and wrong sign electrons and no leptons) assuming a 10 kT Liquid Argon detector with an electron charge confusion of 0.1% . We have computed the exclusion regions in the $\Delta m^2_{12} - \delta$ plane using the Δ_{CP} and Δ_T discriminants, obtaining a similar excluded region provided that the electron detection efficiency is $\sim$20%. The Δm^2_{12} compatible with the LMA solar data can be tested with a flux of 5×10^{21} muons.

• Finally, we have computed the exclusion regions in the $\Delta m^2_{12} - \delta$ plane fitting the visible energy distributions. This method, more powerful than the previous one but not model independent, extends the excluded regions up to values of $|\delta|$ close to π, even when θ_{13} is left free.

References

[1] Y. Fukuda *et al.* (Kamiokande Collaboration), Phys. Lett. B **335**, 237 (1994); R. Becker-Szendy *et al.* (IMB Collaboration), Nucl. Phys. B (Proc. Suppl.) **38**, 331 (1995); S. Fukuda *et al.* (Super-Kamiokande Collaboration), hep-ex/0009001; T. Kajita (Super-Kamiokande Collaboration), Talk presented at NOW2000, Otranto, Italy, September 2000 (http://www.ba.infn.it/~now2000); W.W.M. Allison *et al.* (Soudan 2 Collaboration), Phys. Lett. B **449**, 137 (1999); F. Ronga (MACRO Collaboration), Talk presented at NOW2000, Otranto, Italy, September 2000 (http://www.ba.infn.it/~now2000).

[2] B. Pontecorvo, *J. Expt. Theor. Phys.* **33**, 549 (1957) [Sov. Phys. JETP **6**, 429 (1958)]; B. Pontecorvo, *J. Expt. Theor. Phys.* **34**, 247 (1958) [Sov. Phys. JETP **7**, 172 (1958)]; Z. Maki, M. Nakagawa and S. Sakata, *Prog. Theor. Phys.* **28** (1962) 870; B. Pontecorvo, *J. Expt. Theor. Phys* **53** (1967) 1717; V. Gribov and B. Pontecorvo, Phys. Lett. B **28**, 493 (1969).

[3] "E362 Proposal for a long baseline neutrino oscillation experiment, using KEK-PS and Super-Kamiokande", February 1995.
H. W. Sobel, proceedings of Eighth International Workshop on Neutrino Telescopes, Venice 1999, vol 1 pg 351.

[4] E. Ables *et al.*[MINOS Collaboration], "P-875: A Long baseline neutrino oscillation experiment at Fermilab," FERMILAB-PROPOSAL-P-875.
The MINOS detectors Technical Design Report, NuMI-L-337, October 1998.

[5] K. Kodama *et al.*[OPERA Collaboration], "OPERA: a long baseline ν_τ appearance experiment in the CNGS beam from CERN to Gran Sasso", CERN/SPSC 99-20 SPSC/M635 LNGS-LOI 19/99.

[6] ICARUS Collab., *'ICARUS-II. A Second-Generation Proton Decay Experiment and Neutrino Observatory at the Gran Sasso Laboratory'*, Proposal Vol. I & II, LNGS-94/99, 1994. `ICARUS` Collab. "A first 600 ton `ICARUS` Detector Installed at the Gran Sasso Laboratory", Addendum to proposal, LNGS-95/10 (1995). F. Arneodo *et al.*[ICARUS Collaboration], "Cloning of T600 modules to reach the design sensitive mass", LNGS-EXP 13/89 add. 2/01, Nov. 2001 and references therein. Available at *http://www.cern.ch/icarus*.

[7] F. Arneodo *et al.* [ICARUS collaboration], "The ICARUS experiment, a second-generation proton decay experiment and neutrino observatory at the Gran Sasso laboratory," hep-ex/0103008.

[8] F. Arneodo *et al.* [ICARUS and NOE Collaborations], "ICANOE: Imaging and calorimetric neutrino oscillation experiment: a proposal for a CERN-GS long baseline and atmospheric neutrino oscillation experiment." LNGS-P21/99; CERN/SPSC 99-25; SPSC/P314, September 99.

[9] S. Geer, *Phys. Rev.* D **57**, 1998 (6989)

[10] A. de Rújula, M. B. Gavela and P. Hernández, *Nucl. Phys.* B **547**, 1999 (21); V. Barger, S. Geer, R. Raja and K. Whisnant, Phys. Rev. **D62**, 013004 (2000) [hep-ph/9911524]; Phys. Rev. **D62**, 073002 (2000) [hep-ph/0003184]; A. Bueno, M. Campanelli and A. Rubbia, Nucl. Phys. **B573** (2000) 27; V. Barger, S. Geer and K. Whisnant, *Phys. Rev.* D **61**, 2000 (053004); M. Freund, M. Lindner, S. T. Petcov and A. Romanimo, Nucl. Phys. **B578**, 27 (2000) [hep-ph/9912457]; A. Cervera *et al.*, Nucl. Phys. **B579**, 17 (2000) [hep-ph/0002108].

[11] A. Bueno, M. Campanelli and A. Rubbia, hep-ph/9809252; CERN-EP/98-140.

[12] M. Apollonio *et al.*[CHOOZ Collaboration], *Phys. Lett.* B **466**, 1999 (415) *Phys. Lett.* B **420**, 1998 (397)

[13] A. Cervera *et al.*, Nucl. Phys. **B579**, 17 (2000) [hep-ph/0002108].

[14] Information on the neutrino factory studies and mu collider collaboration at BNL can be found at *http://www.cap.bnl.gov/mumu/*
Information on the neutrino factory studies at FNAL can be found at *http://www.fnal.gov/projects/muon_collider/*
Information on the neutrino factory studies at CERN can be found at *http://muonstoragerings.cern.ch/Welcome.html/*

[15] A. Cervera, A. Donini, M. B. Gavela, J. J. Gomez Cadenas, P. Hernandez, O. Mena and S. Rigolin, Nucl. Phys. B **579**, 17 (2000) [hep-ph/0002108].

[16] P. Lipari, "CP violation effects and high energy neutrinos", hep-ph/0102046.

[17] A. Bueno, M. Campanelli and A. Rubbia, Nucl. Phys. B **589**, 577 (2000) [hep-ph/0005007].

[18] T. Ota and J. Sato, "Matter profile effect in neutrino factory", hep-ph/0011234.

[19] M. Koike and J. Sato, Phys. Rev. D **61**, 073012 (2000) [hep-ph/9909469].

[20] J. Arafune, M. Koike and J. Sato, Phys. Rev. D **56**, 3093 (1997) [hep-ph/9703351]. J. Arafune and J. Sato, Phys. Rev. D **55**, 1653 (1997)

[21] J. Sato, "CP and T violation in (long) long baseline neutrino oscillation experiments", hep-ph/9910442.

[22] H. W. Zaglauer and K. H. Schwarzer, *Z. Phys.* C **40**, 1988 (273)

[23] V. Barger, K. Whisnant, S. Pakvasa and R. J. N. Phillips, *Phys. Rev.* D **22**, 1980 (2718)

[24] P. Lipari, Phys. Rev. D **61**, 113004 (2000) [hep-ph/9903481].

[25] P. F. Harrison and W. G. Scott, Phys. Lett. B **476**, 349 (2000) [hep-ph/9912435].

[26] A. Romanino, Nucl.Phys. B **574** 675-690 (2000) [hep-ph/9909425]

[27] A. Rubbia *et al.*, talk given at NUINT01, KEK (Japan), Dec. 2001.

[28] A. Bueno, M. Campanelli and A. Rubbia, hep-ph/9808485 ETHZ-IPP-98-05.

[29] S. Navas *et al.*, "Prospects for CP and T violation measurements with a magnetized Liquid Argon detector", talk given at the Workshop on a Massive Underground Neutrino Detector with Leptonic Charge-Sign Discrimination, Sitges (Spain), Nov. 2001. A. Rubbia, "Neutrino factories: Detector concepts for studies of CP and T violation effects in neutrino oscillations," arXiv:hep-ph/0106088, talk given at 9th International Symposium on Neutrino Telescopes, Venice (Italy), March 2001.

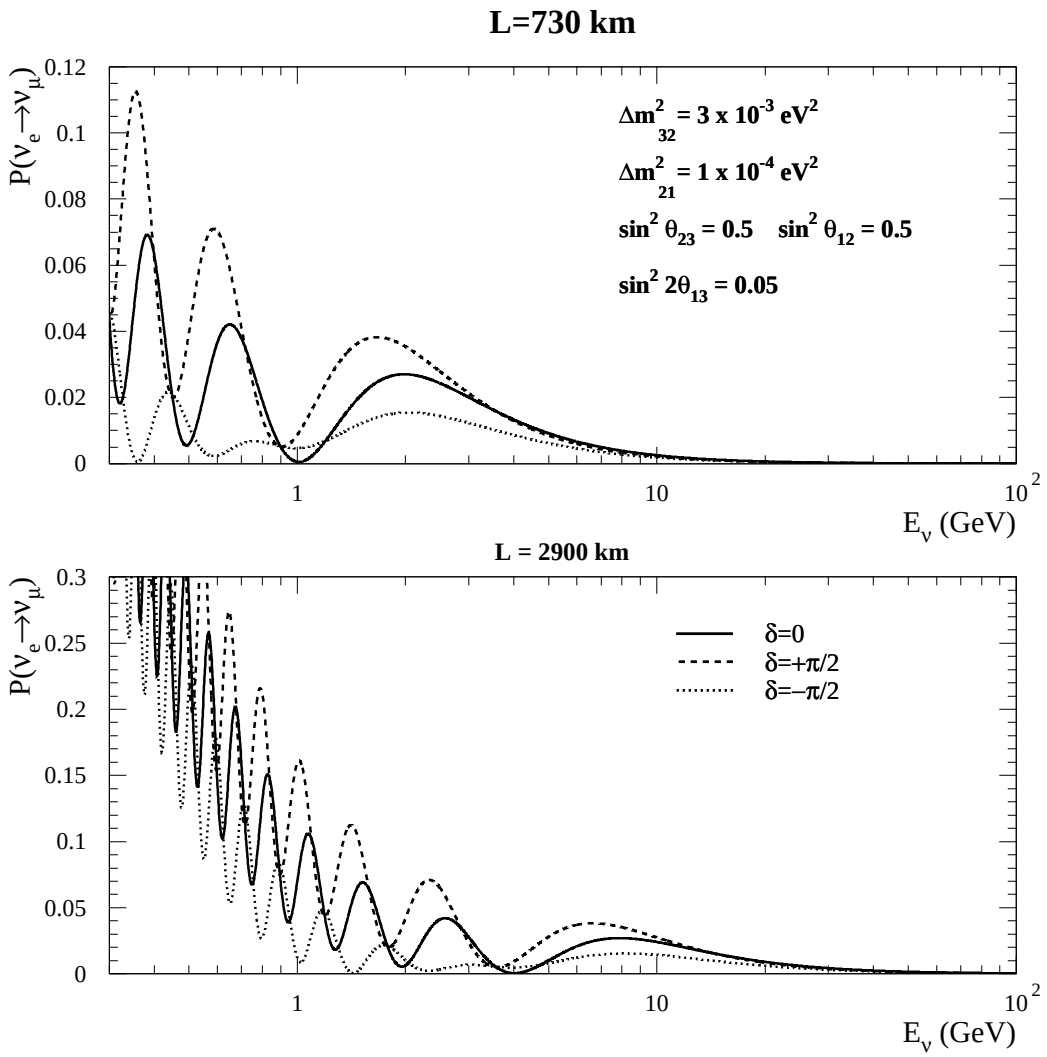

Figure 1: Probability for $\nu_e \to \nu_\mu$ oscillations in vacuum for two baselines $L = 730$ km and 2900 km as a function of neutrino energy E_ν. The probabilities are computed for three values of the δ-phase: $\delta = 0$ (line), $\delta = +\pi/2$ (dashed), $\delta = -\pi/2$ (dotted). The other oscillation parameters are $\Delta m^2_{32} = 3 \times 10^{-3}$ eV^2, $\Delta m^2_{21} = 1 \times 10^{-4}$ eV^2, $\sin^2\theta_{23} = 0.5$, $\sin^2\theta_{12} = 0.5$, and $\sin^2 2\theta_{13} = 0.05$.

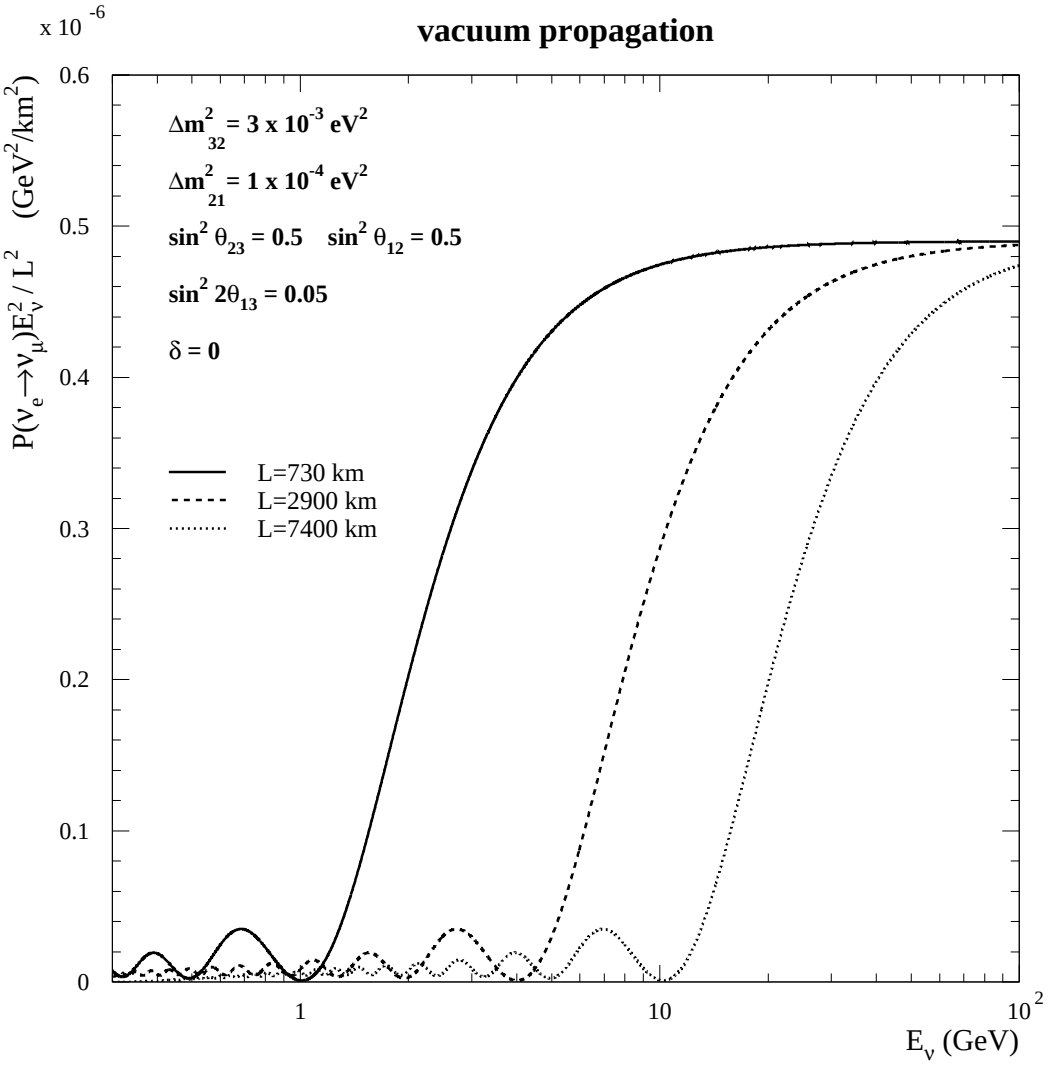

Figure 2: Rescaled probability (see text) for $\nu_e \to \nu_\mu$ oscillations in vacuum for three baselines $L = 730$ km (line), 2900 km (dashed) and 7400 km (dotted) as a function of neutrino energy E_ν. The oscillation parameters are $\Delta m^2_{32} = 3 \times 10^{-3}$ eV^2, $\Delta m^2_{21} = 1 \times 10^{-4}$ eV^2, $\sin^2\theta_{23} = 0.5$, $\sin^2\theta_{12} = 0.5$, $\sin^2 2\theta_{13} = 0.05$ and $\delta = 0$.

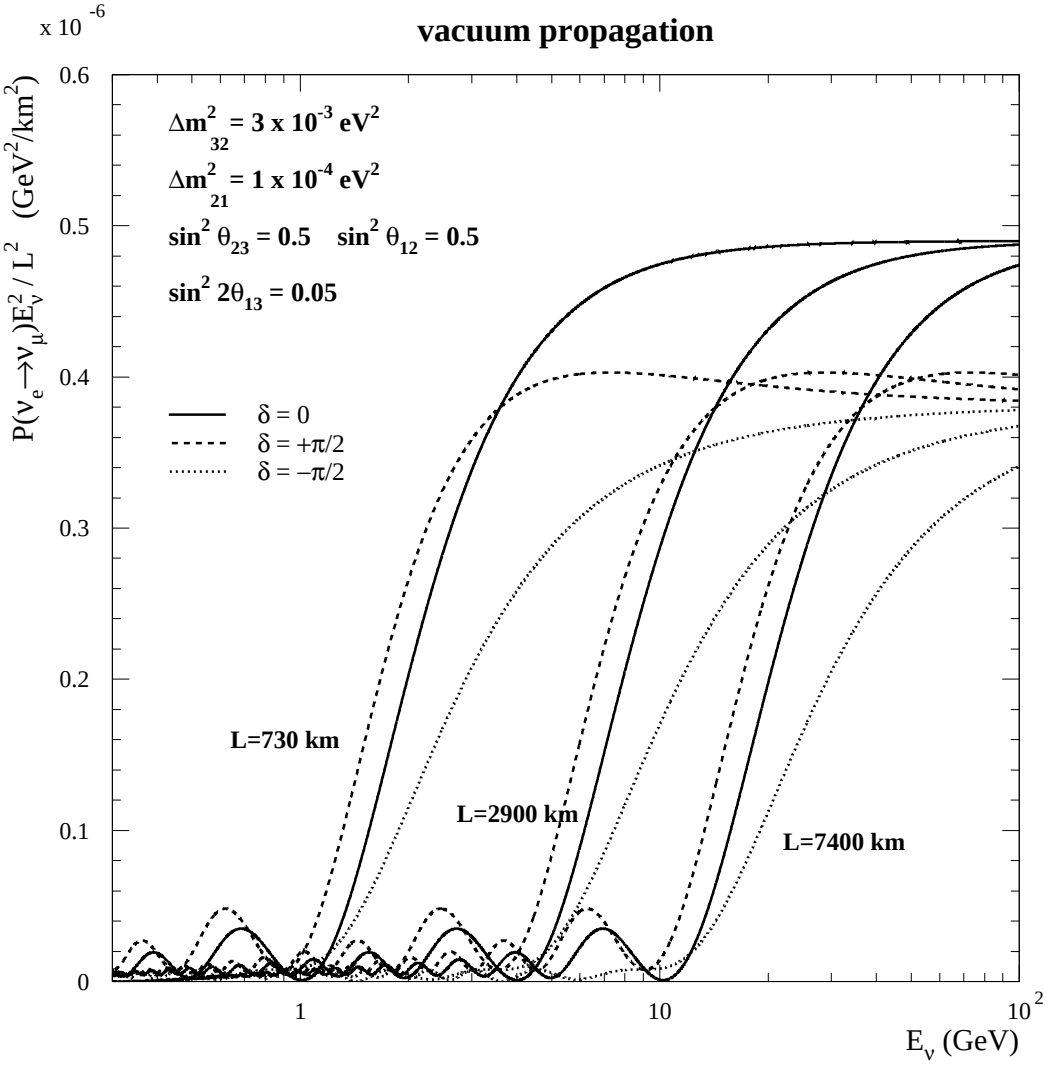

Figure 3: Rescaled probability (see text) for $\nu_e \to \nu_\mu$ oscillations in vacuum for three baselines $L = 730$ km (line), 2900 km (dashed) and 7400 km (dotted) as a function of neutrino energy E_ν. For each baseline, the probabilities are computed for three values of the δ-phase: $\delta = 0$ (upper), $\delta = +\pi/2$ (middle), $\delta = -\pi/2$ (lower). The oscillation parameters are $\Delta m^2_{32} = 3 \times 10^{-3}$ eV^2, $\Delta m^2_{21} = 1 \times 10^{-4}$ eV^2, $\sin^2\theta_{23} = 0.5$, $\sin^2\theta_{12} = 0.5$, $\sin^2 2\theta_{13} = 0.05$.

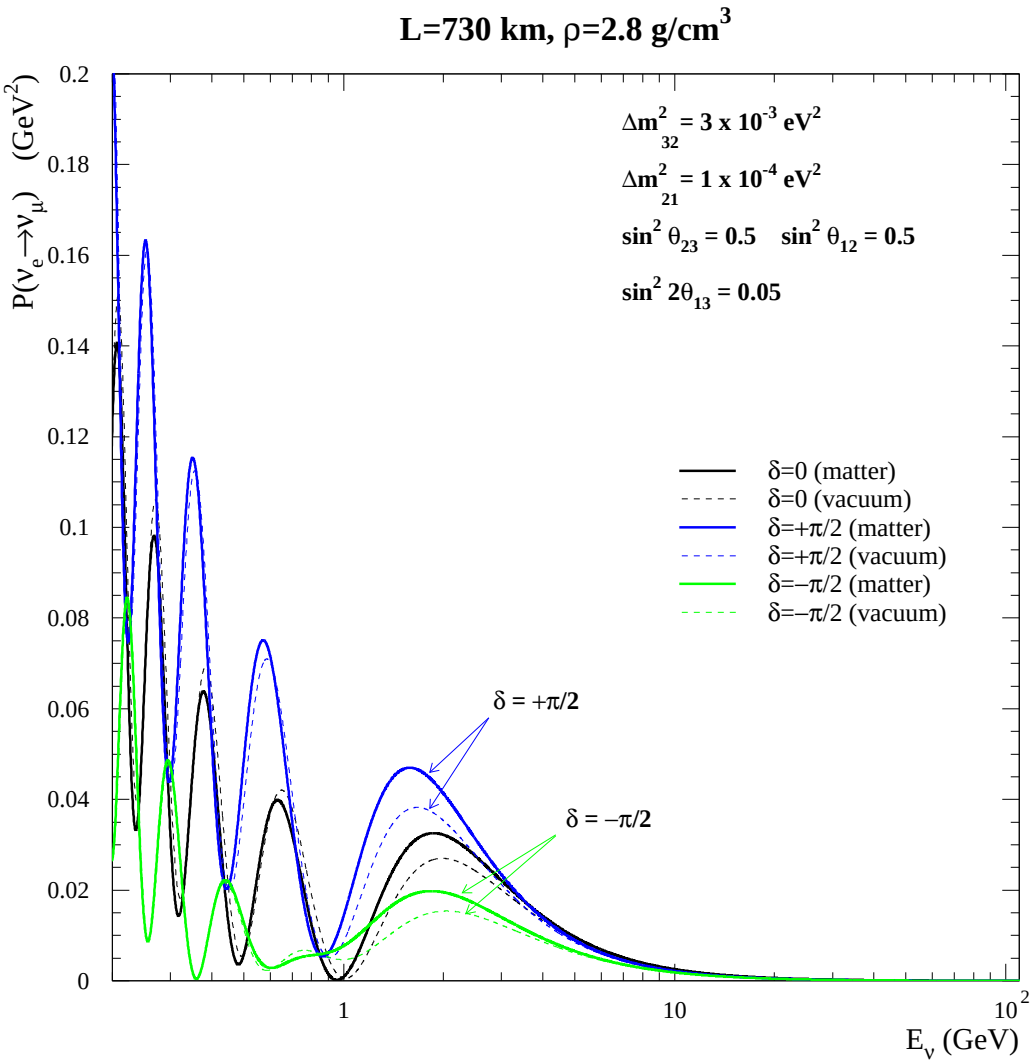

Figure 4: Oscillation probability for $\nu_e \to \nu_\mu$ oscillations for a baseline $L = 730$ km as a function of neutrino energy E_ν. The probabilities are computed for neutrinos in matter (full line) and in vacuum (dotted line) and for three values of the δ-phase: $\delta = 0$, $\delta = +\pi/2$ and $\delta = -\pi/2$. The oscillation parameters are $\Delta m^2_{32} = 3 \times 10^{-3}$ eV^2, $\Delta m^2_{21} = 1 \times 10^{-4}$ eV^2, $\sin^2\theta_{23} = 0.5$, $\sin^2\theta_{12} = 0.5$, $\sin^2 2\theta_{13} = 0.05$.

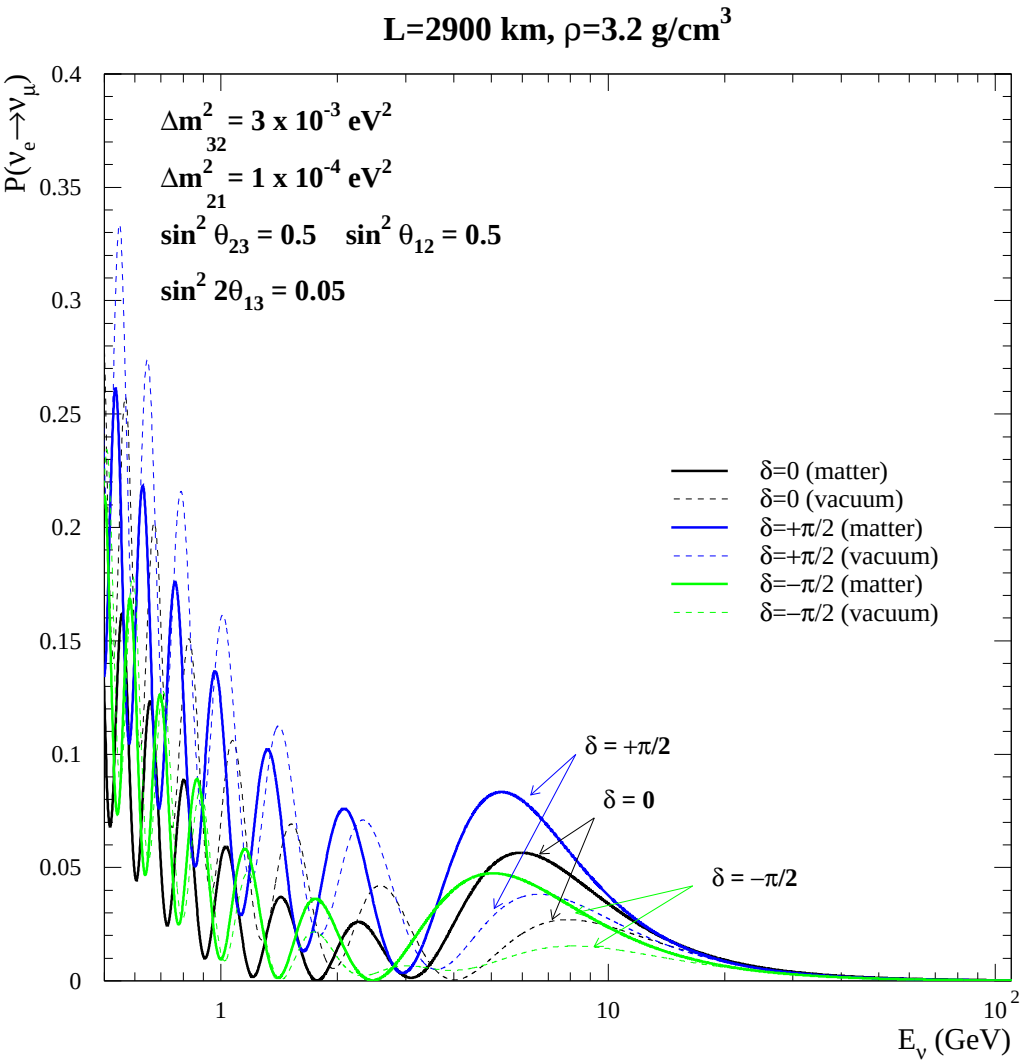

Figure 5: Same as Figure 4 but for a baseline $L = 2900$ km.

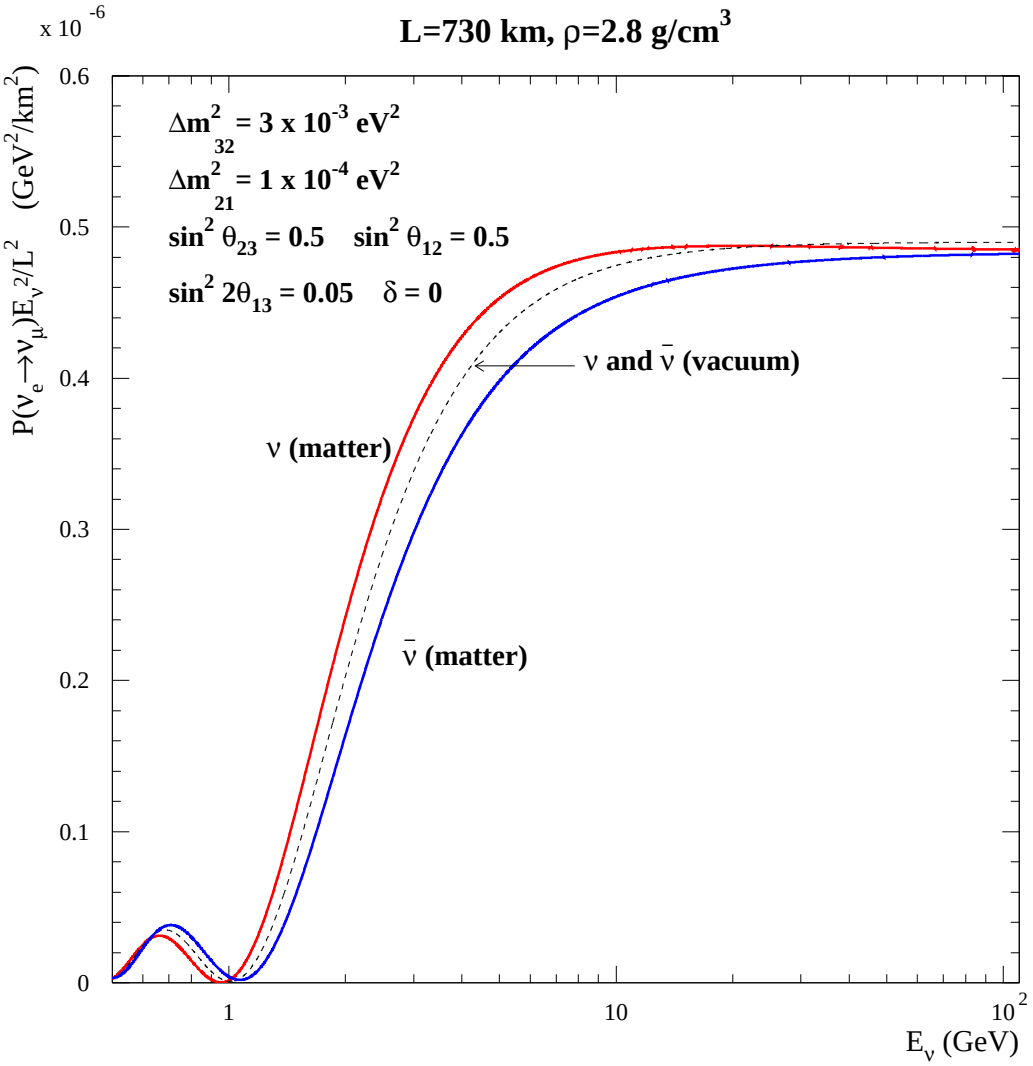

Figure 6: Rescaled probability (see text) for $\nu_e \rightarrow \nu_\mu$ oscillations for a baseline $L = 730$ km as a function of neutrino energy E_ν. The probabilities are computed for neutrinos in matter, in vacuum (dotted line, same for neutrinos and antineutrinos) and for antineutrinos in matter. The oscillation parameters are $\Delta m^2_{32} = 3 \times 10^{-3}$ eV^2, $\Delta m^2_{21} = 1 \times 10^{-4}$ eV^2, $\sin^2\theta_{23} = 0.5$, $\sin^2\theta_{12} = 0.5$, $\sin^2 2\theta_{13} = 0.05$ and $\delta = 0$.

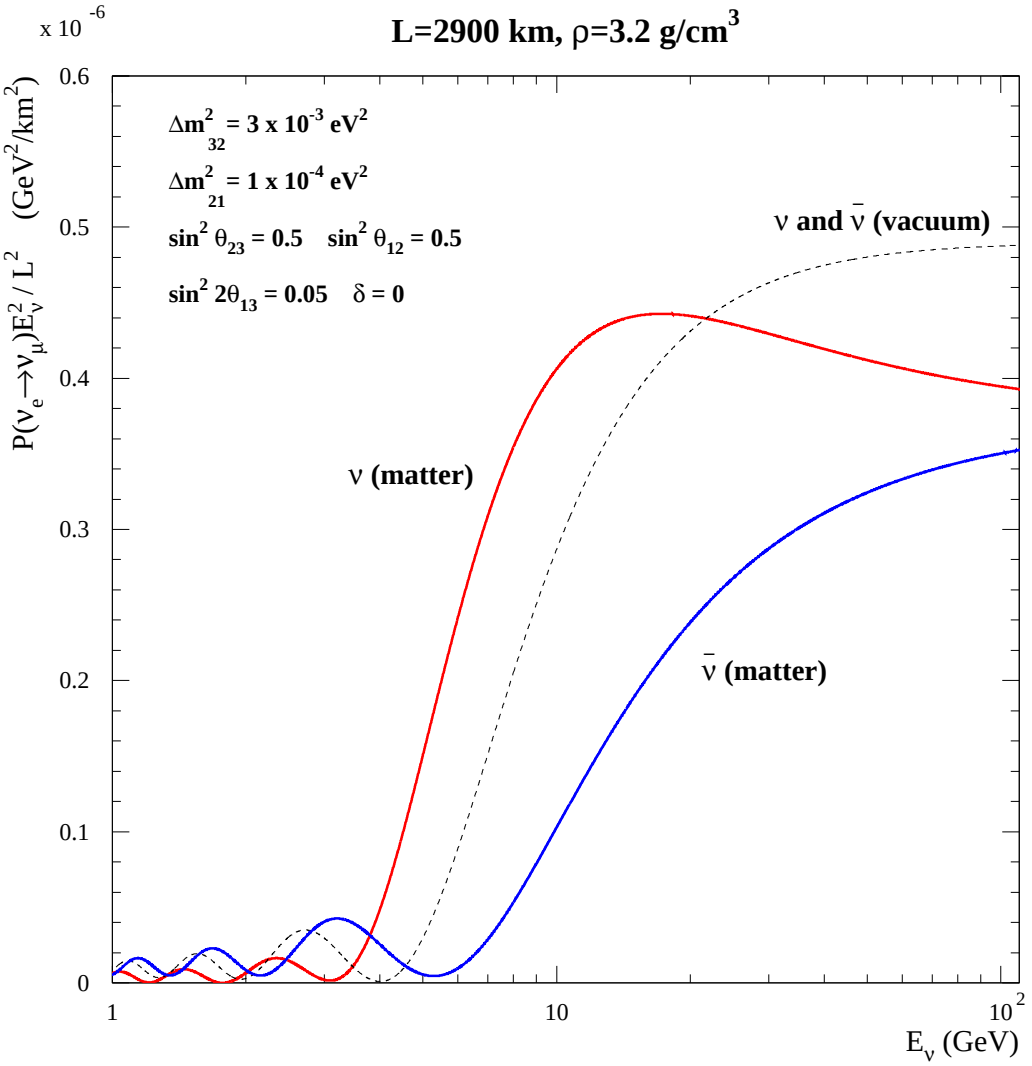

Figure 7: Same as Figure 6 but for a baseline $L = 2900$ km.

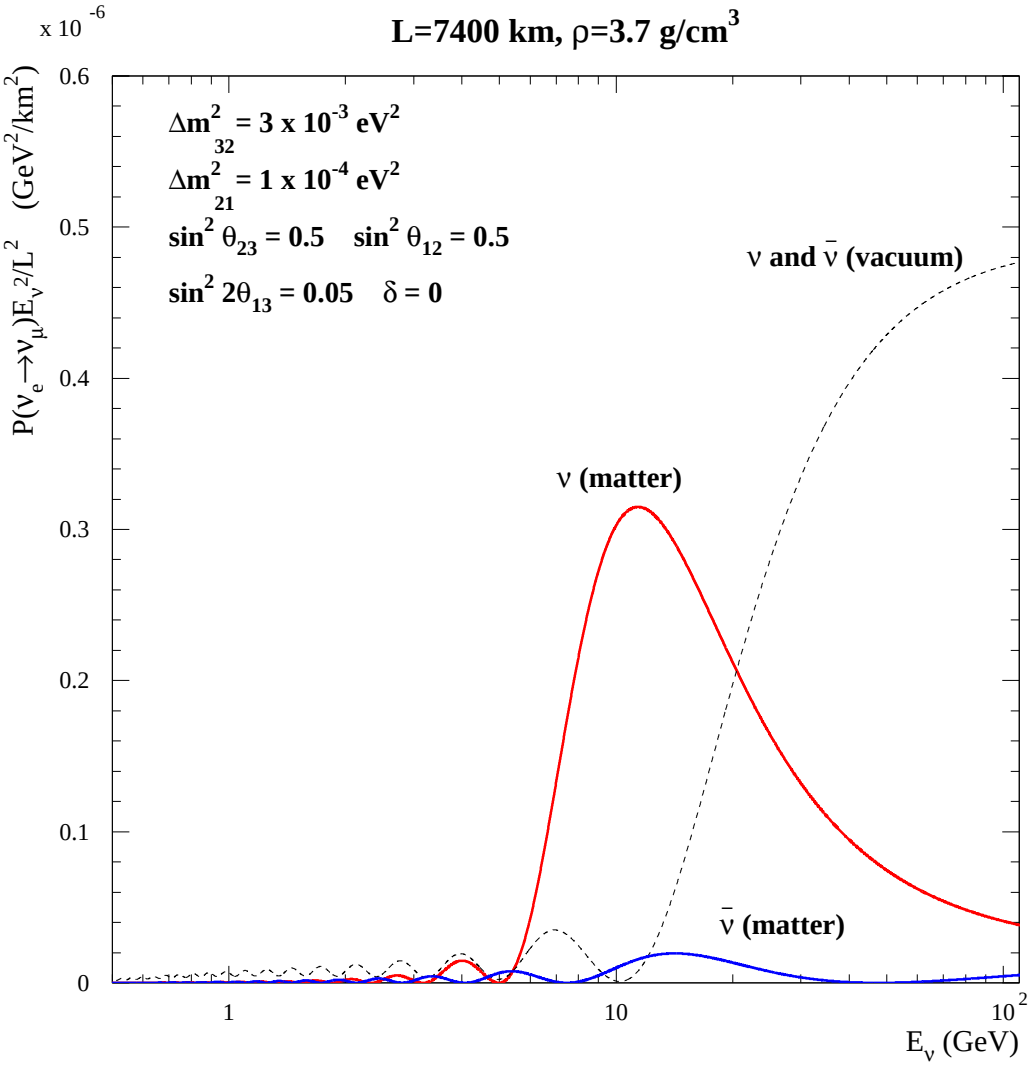

Figure 8: Same as Figure 6 but for a baseline $L = 7400$ km.

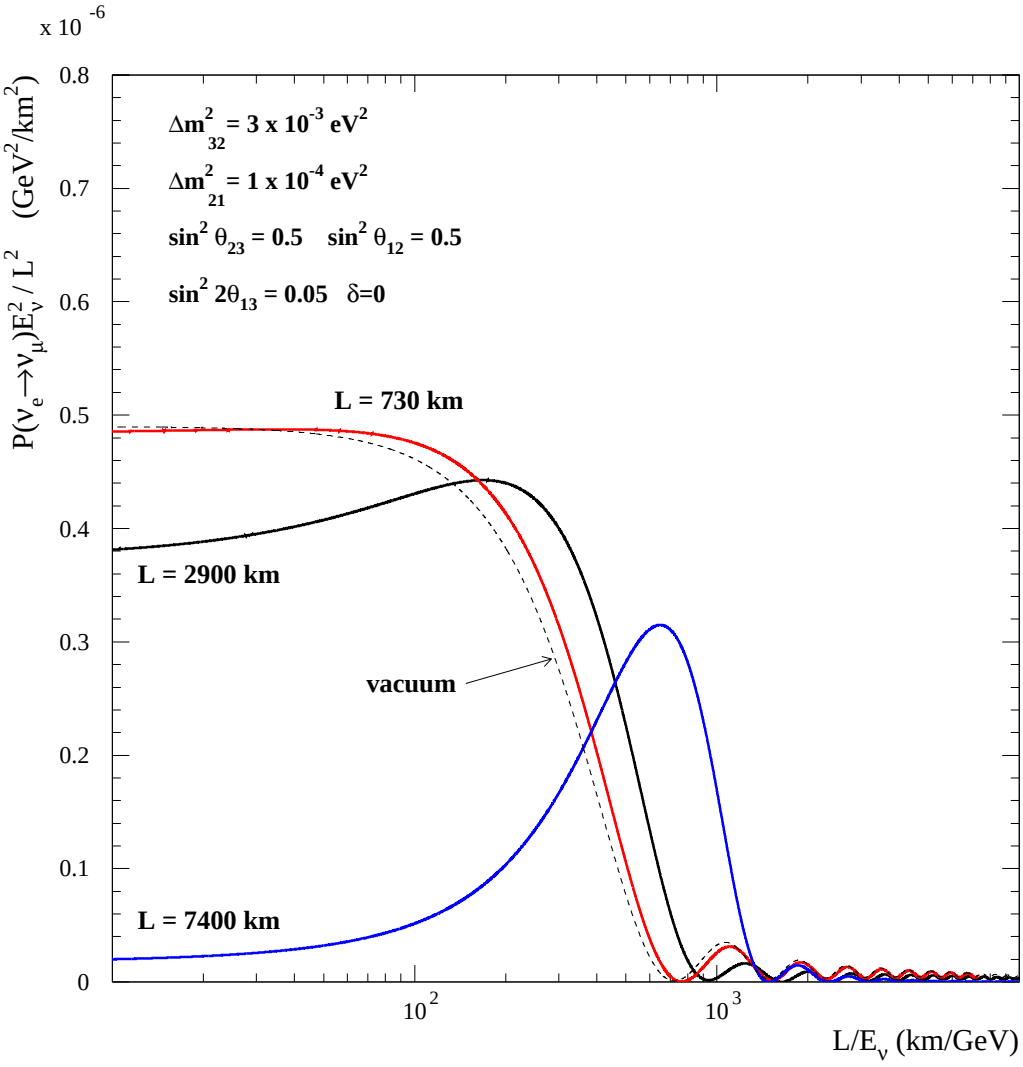

Figure 9: Same as plots in Figure 6 but only for neutrinos and as a function of L/E_ν for three baselines $L = 730$ km, 2900 km, 7400 km and in vacuum (dashed line, independent of baseline). The oscillation parameters are $\Delta m^2_{32} = 3\times10^{-3}$ eV^2, $\Delta m^2_{21} = 1\times10^{-4}$ eV^2, $\sin^2\theta_{23} = 0.5$, $\sin^2\theta_{12} = 0.5$, $\sin^2 2\theta_{13} = 0.05$ and $\delta = 0$.

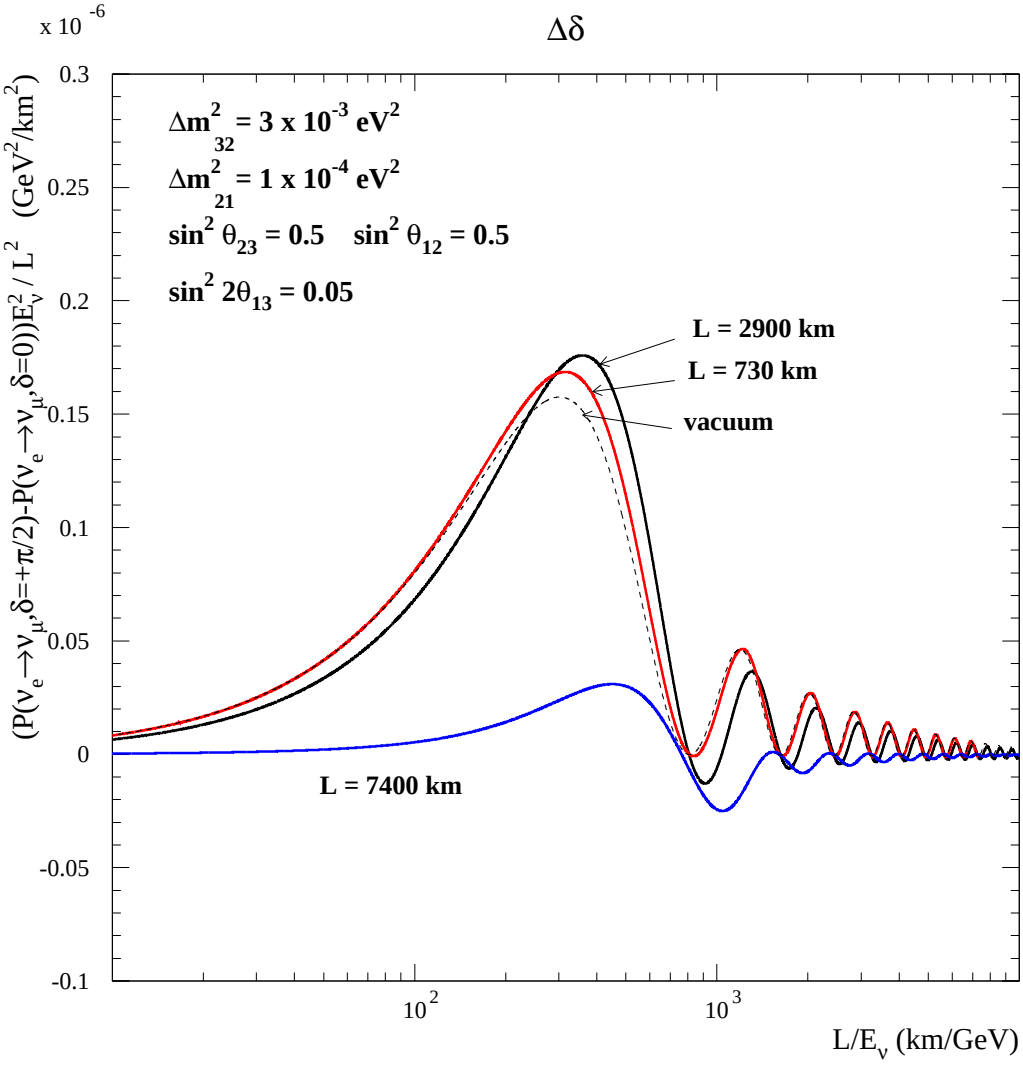

Figure 10: The rescaled Δ_δ discriminant (see text for definition) as a function of the L/E_ν ratio, computed for neutrinos propagating in matter at three different baselines $L = 730$ km, 2900 km and 7400 km (full lines), and for neutrinos propagating in vacuum (dashed line).

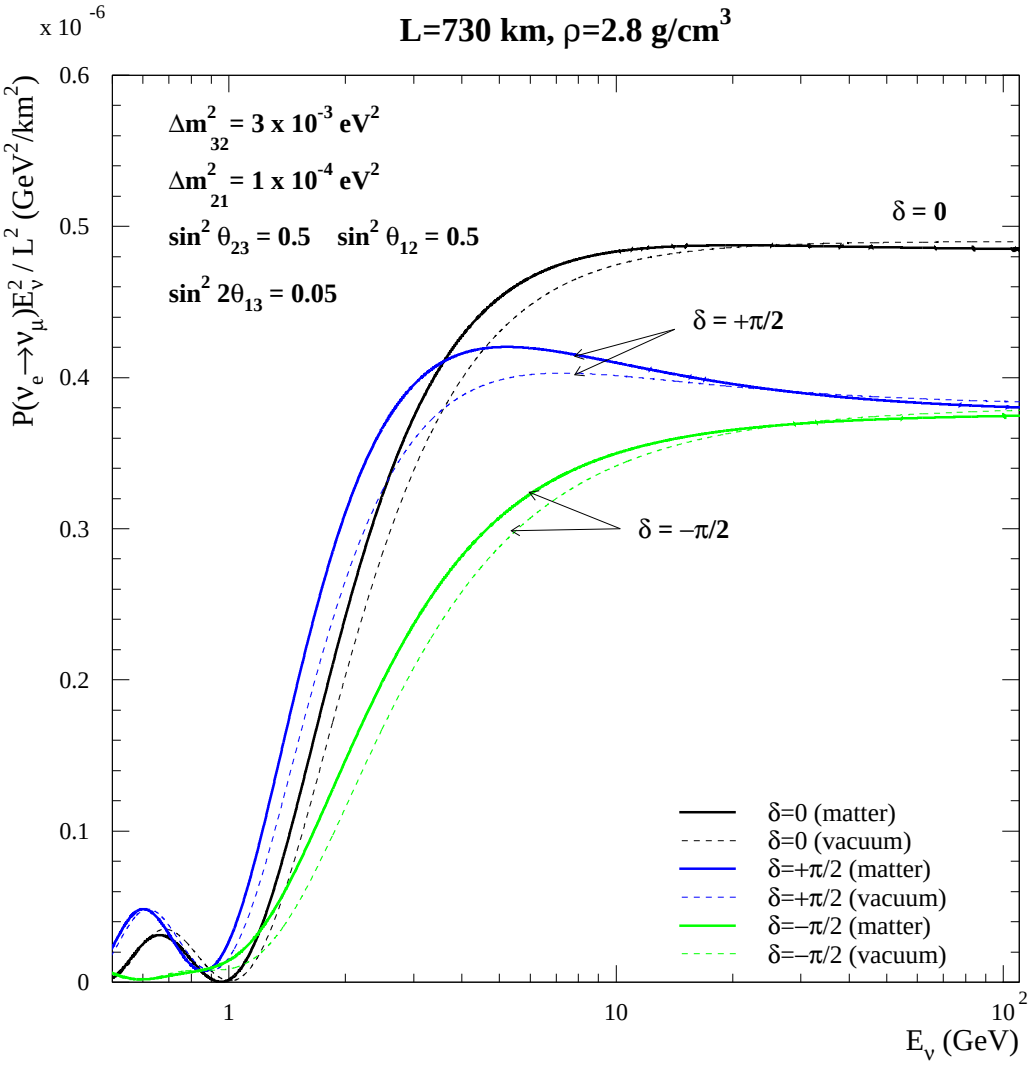

Figure 11: Rescaled probability (see text) for $\nu_e \to \nu_\mu$ oscillations for a baseline $L = 730$ km as a function of neutrino energy E_ν. The probabilities are computed for neutrinos in matter (full line) and in vacuum (dotted line), and for three values of the δ-phase: $\delta = 0$, $\delta = +\pi/2$, $\delta = -\pi/2$. The other oscillation parameters are $\Delta m^2_{32} = 3 \times 10^{-3}$ eV^2, $\Delta m^2_{21} = 1 \times 10^{-4}$ eV^2, $\sin^2\theta_{23} = 0.5$, $\sin^2\theta_{12} = 0.5$, $\sin^2 2\theta_{13} = 0.05$.

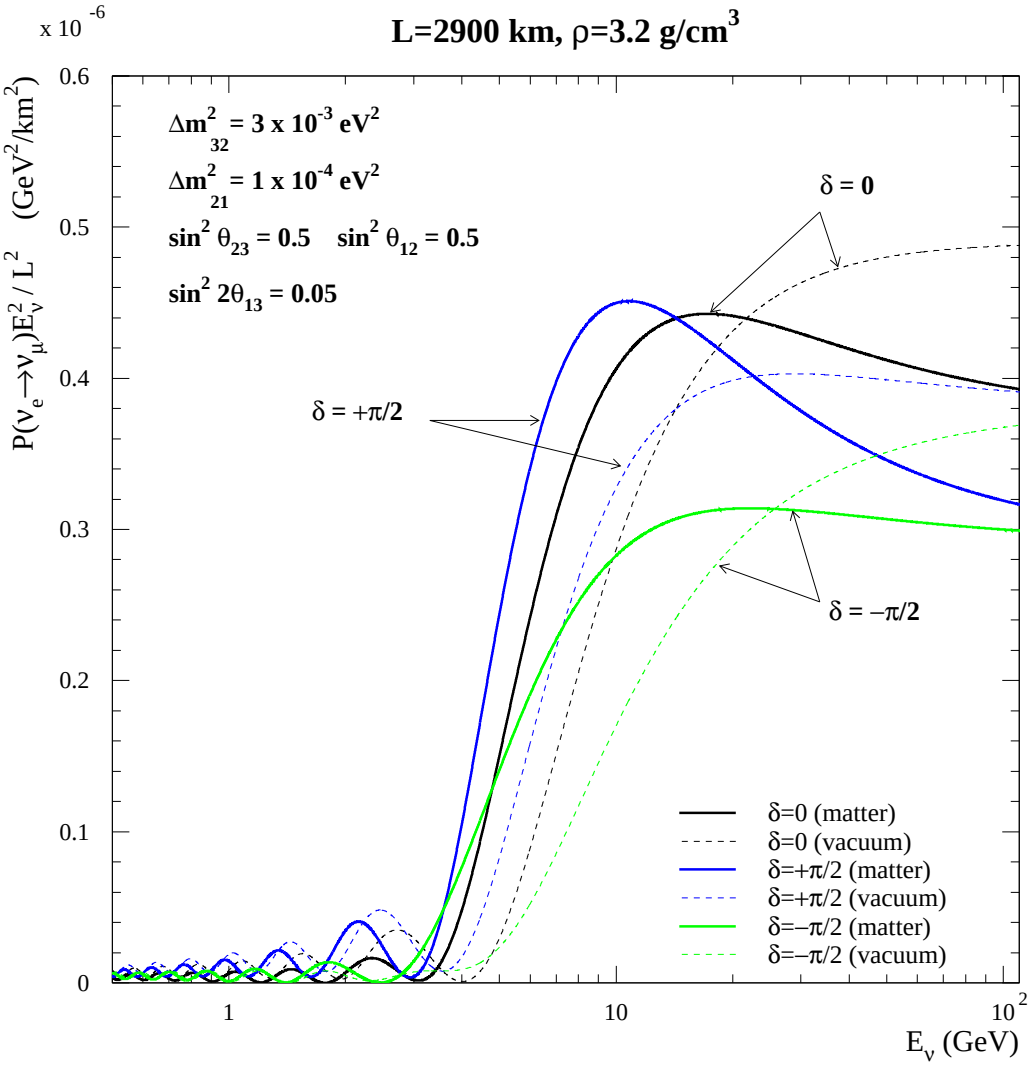

Figure 12: Same as Figure 11 but for a baseline $L = 2900$ km.

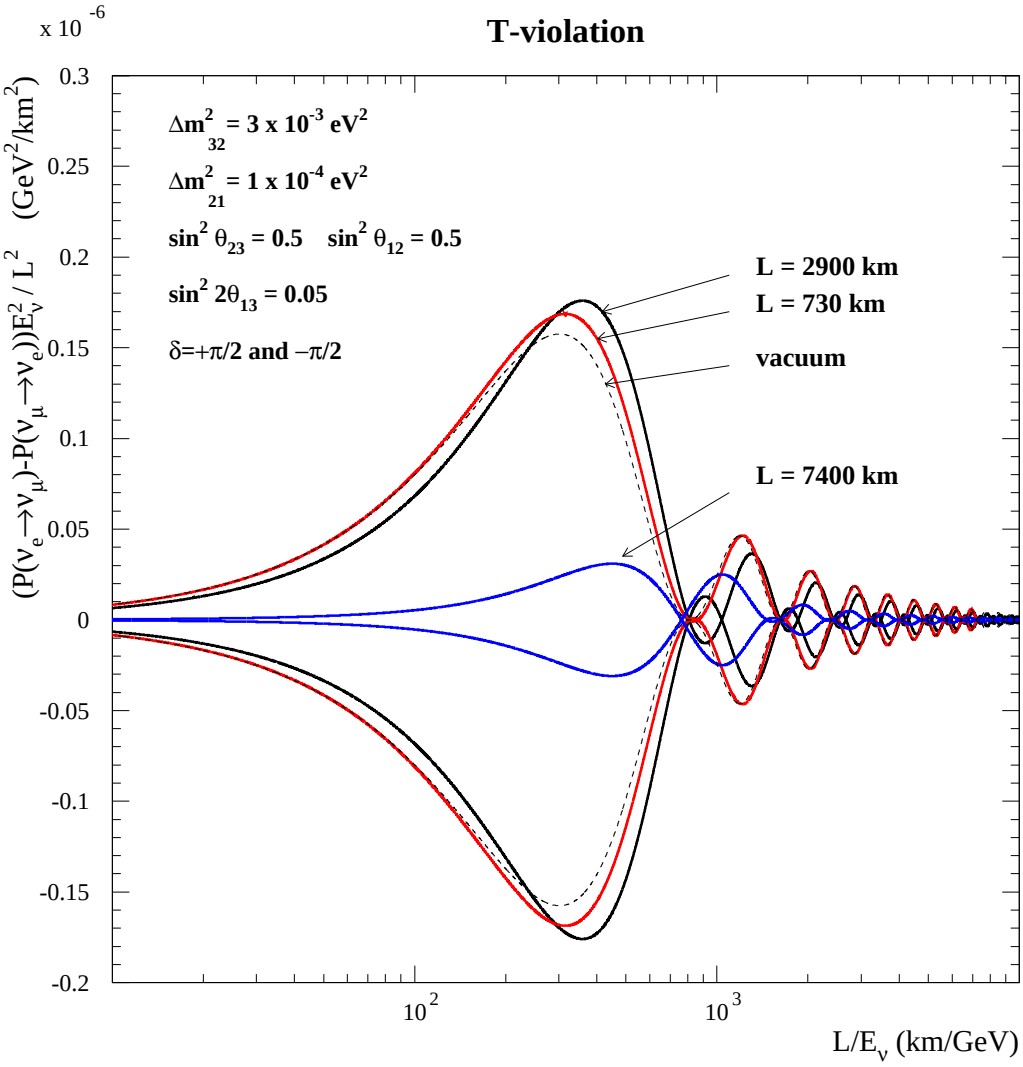

Figure 13: The rescaled Δ_T discriminant (see text for definition) as a function of the L/E_ν ratio, computed for neutrinos propagating in matter at three different baselines $L = 730$ km, 2900 km and 7400 km, and also for propagation vacuum (independent of baseline). Two sets of curves are represented, corresponding to $\delta = +\pi/2$ (upper ones) and $\delta = -\pi/2$ (lower ones). The other oscillation parameters are $\Delta m^2_{32} = 3 \times 10^{-3}$ eV^2, $\Delta m^2_{21} = 1 \times 10^{-4}$ eV^2, $\sin^2\theta_{23} = 0.5$, $\sin^2\theta_{12} = 0.5$ and $\sin^2 2\theta_{13} = 0.05$.

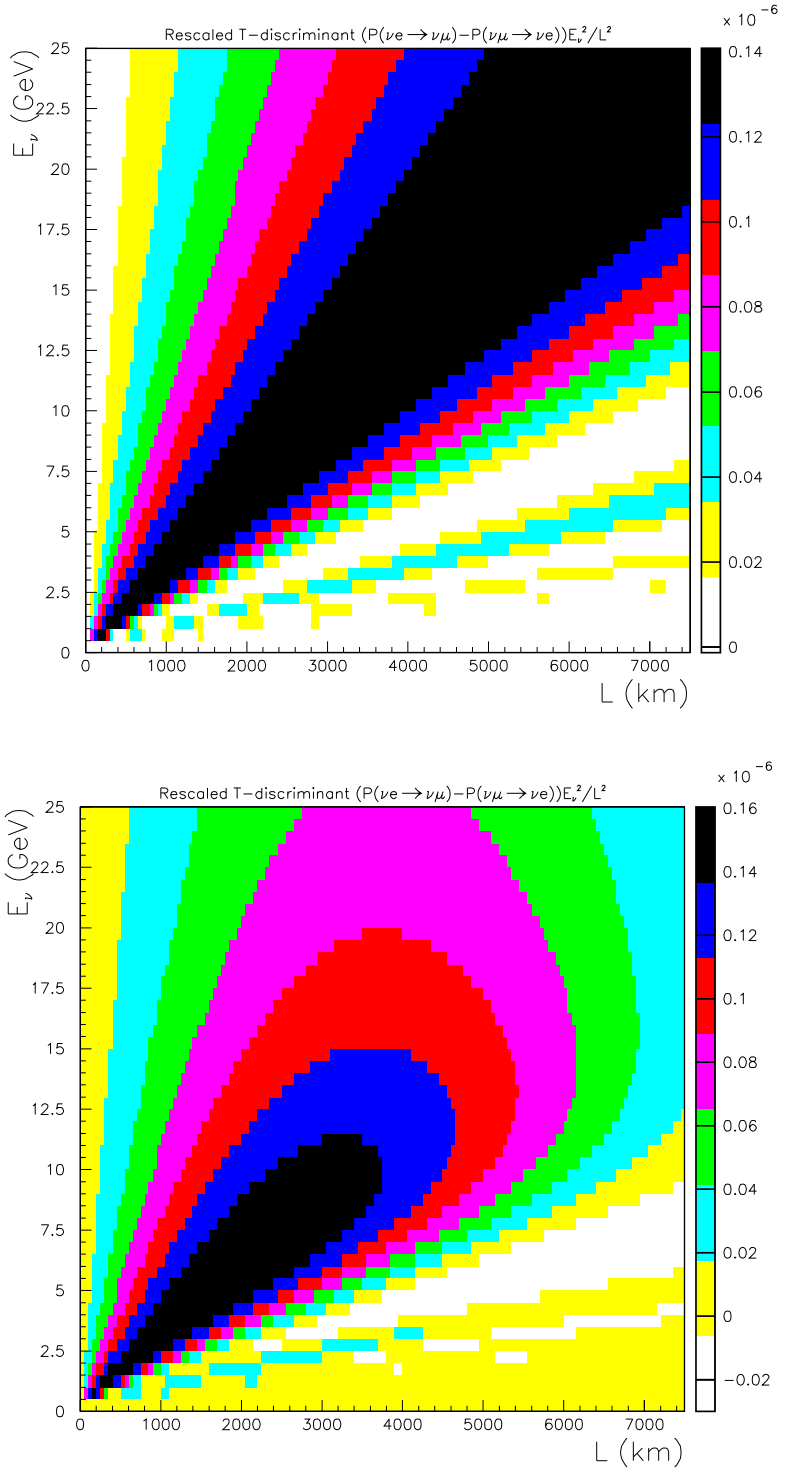

Figure 14: The rescaled Δ_T discriminant (see text for definition) as a function of the L and E_ν, computed for neutrinos propagating in vacuum (upper) and in matter (lower) for $\delta = \pi/2$. The other oscillation parameters are $\Delta m^2_{32} = 3 \times 10^{-3}$ eV^2, $\Delta m^2_{21} = 1 \times 10^{-4}$ eV^2, $\sin^2\theta_{23} = 0.5$, $\sin^2\theta_{12} = 0.5$ and $\sin^2 2\theta_{13} = 0.05$.

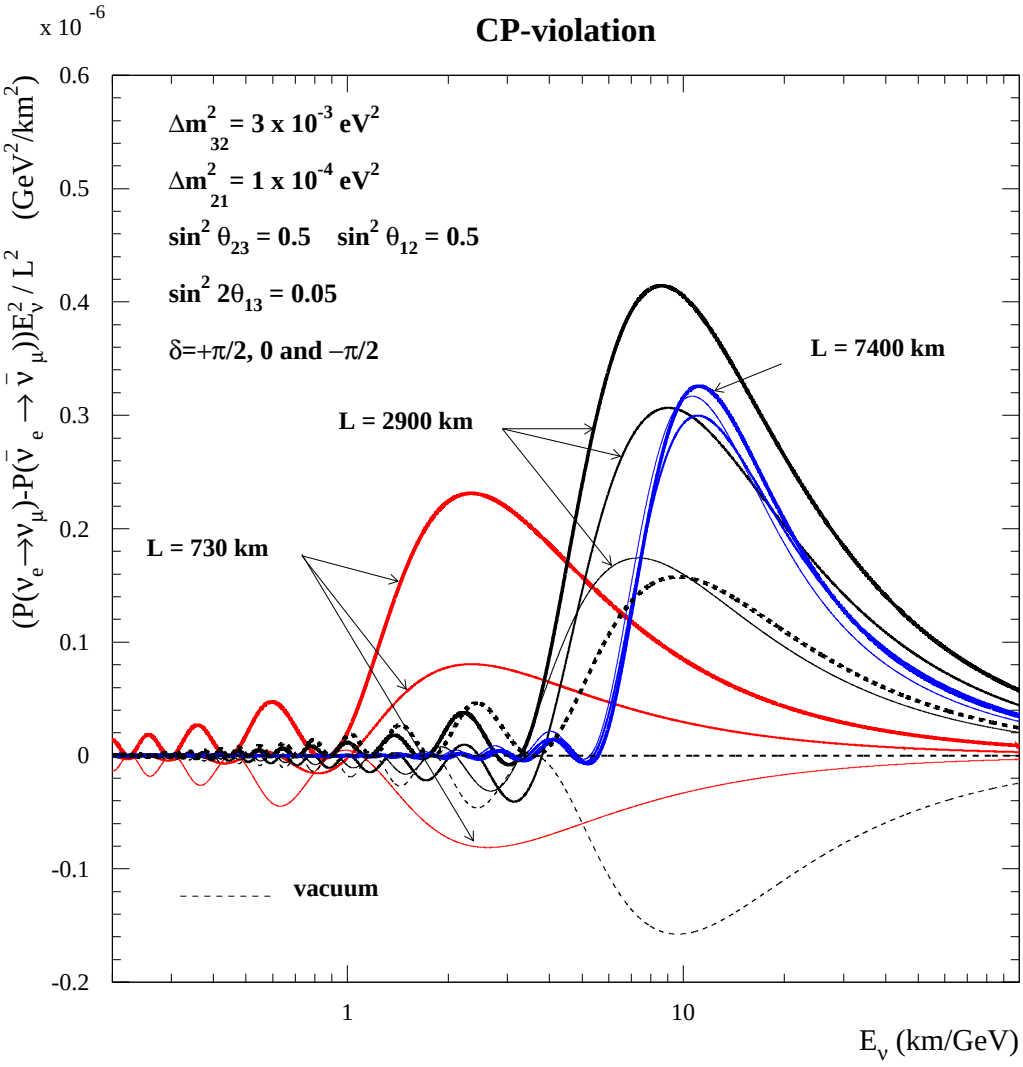

Figure 15: The rescaled Δ_{CP} discriminant (see text for definition) as a function of the neutrino energy E_ν, computed for neutrinos propagating in matter at three different baselines $L = 730$ km, 2900 km and 7400 km. Three sets of curves are represented, corresponding to $\delta = +\pi/2$ (thick lines), $\delta = -\pi/2$ (thin lines) and $\delta = 0$. The other oscillation parameters are $\Delta m^2_{32} = 3 \times 10^{-3}$ eV^2, $\Delta m^2_{21} = 1 \times 10^{-4}$ eV^2, $\sin^2\theta_{23} = 0.5$, $\sin^2\theta_{12} = 0.5$ and $\sin^2 2\theta_{13} = 0.05$.

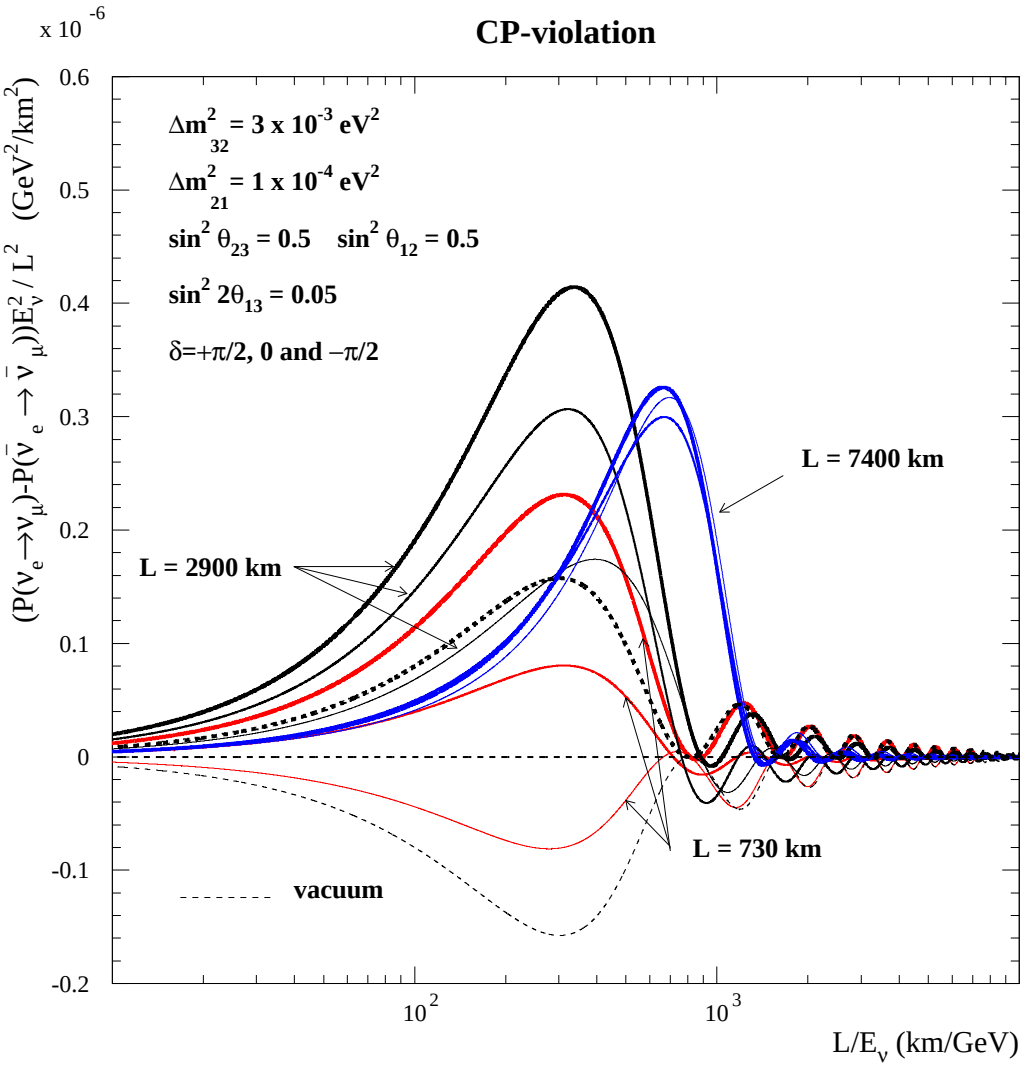

Figure 16: Same as Figure 15 but as a function of the L/E_ν ratio. In addition to the three different baselines, the case of neutrinos propagating in vacuum (independent of baseline) is also shown for comparison.

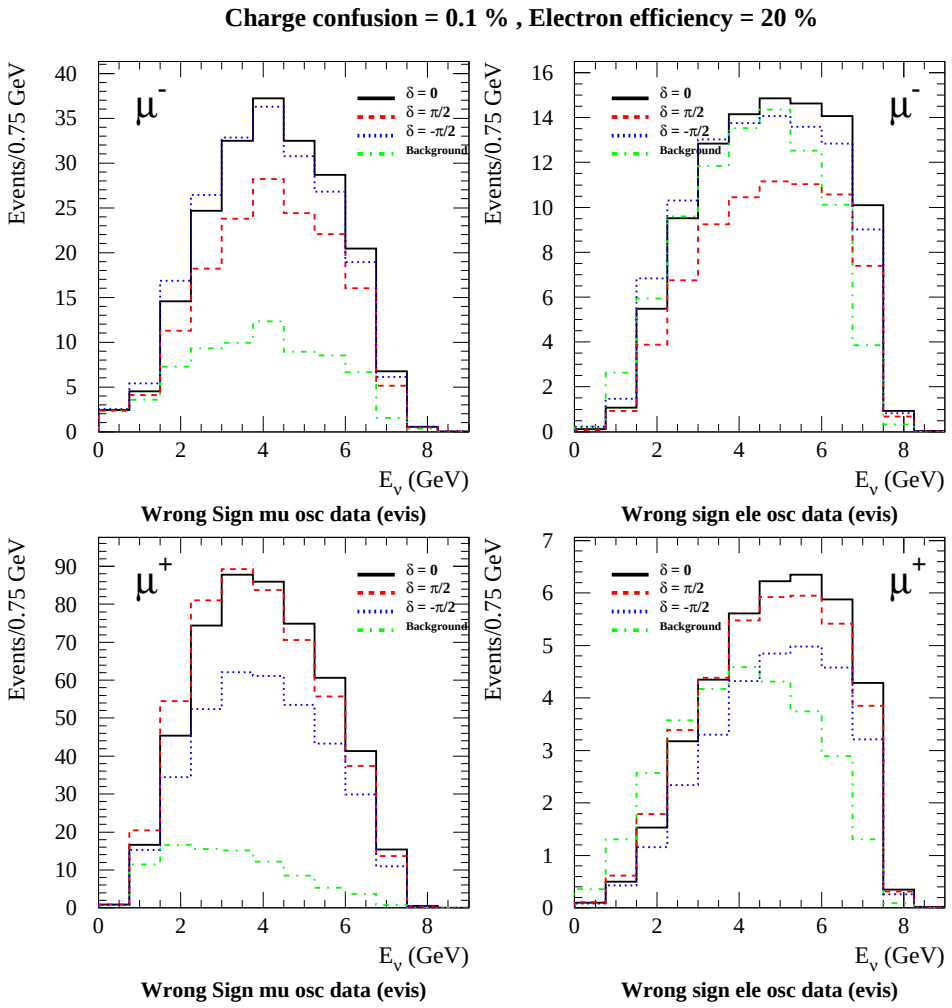

Figure 17: Visible energy distribution for wrong-sign muons (left) and wrong-sign electrons (right) normalized to 10^{21} muon decays. The electron efficiency ϵ_e is assumed to be 20% and charge confusion probability is set to 0.1%. Three sets of curves are represented, corresponding to $\delta = +\pi/2$ (dashed line), $\delta = 0$ (full line) and $\delta = -\pi/2$ (dotted line). The background contribution from tau decays is also shown. The other oscillation parameters are $\Delta m^2_{32} = 3 \times 10^{-3}$ eV^2, $\Delta m^2_{21} = 1 \times 10^{-4}$ eV^2, $\sin^2\theta_{23} = 0.5$, $\sin^2\theta_{12} = 0.5$ and $\sin^2 2\theta_{13} = 0.05$.

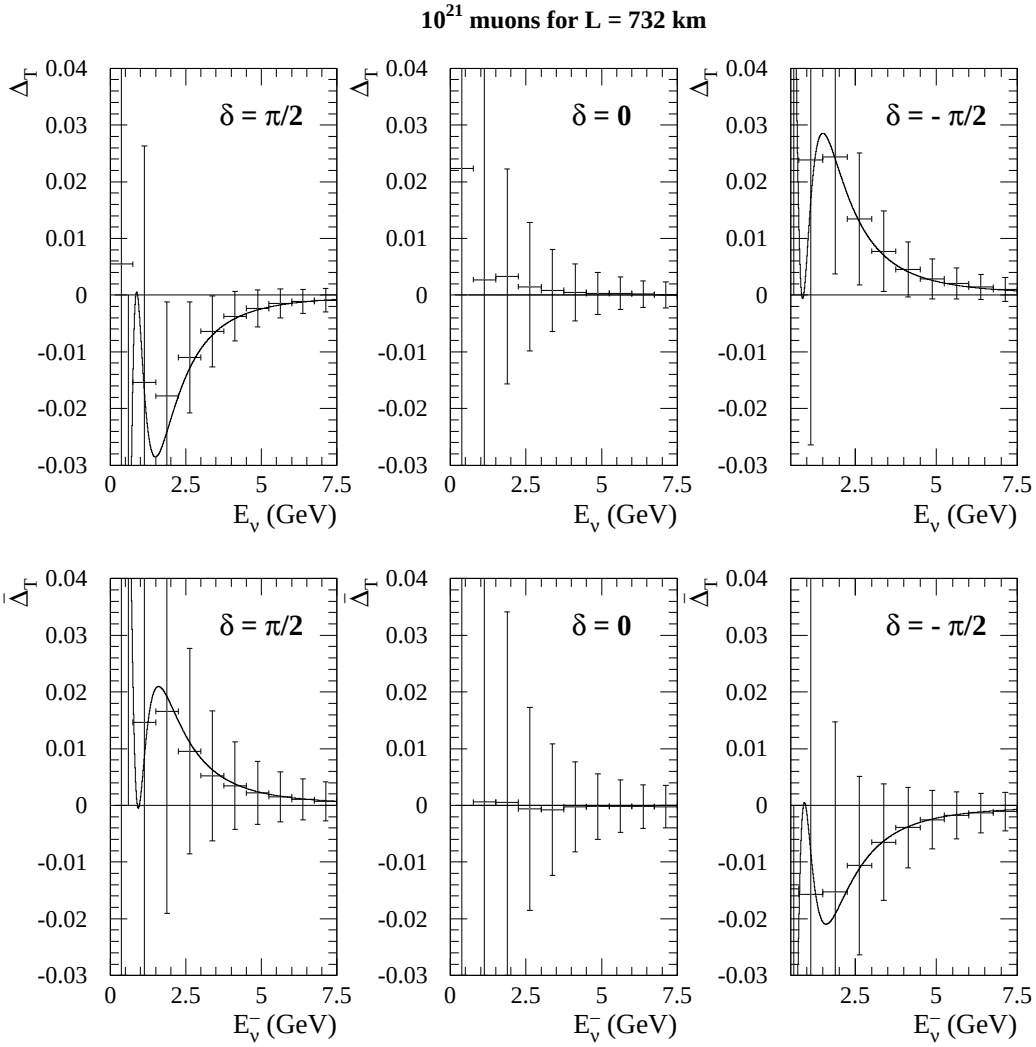

Figure 18: Direct T-violation: Binned $\Delta_T(i)$ discriminant for neutrinos (upper plots) and antineutrinos (lower plots) for three values of the δ-phase: $\delta = +\pi/2$, $\delta = 0$ and $\delta = -\pi/2$. The errors are statistical and correspond to a normalization of 10^{21} muon decays and a baseline of $L = 732$ km. A 20% electron efficiency with a charge confusion probability of 0.1% has been assumed. The change of sign of the effect with respect of the change $\delta \to -\delta$ and the substitution of neutrinos by antineutrinos is clearly visible. The full curve corresponds to the theoretical probability difference.

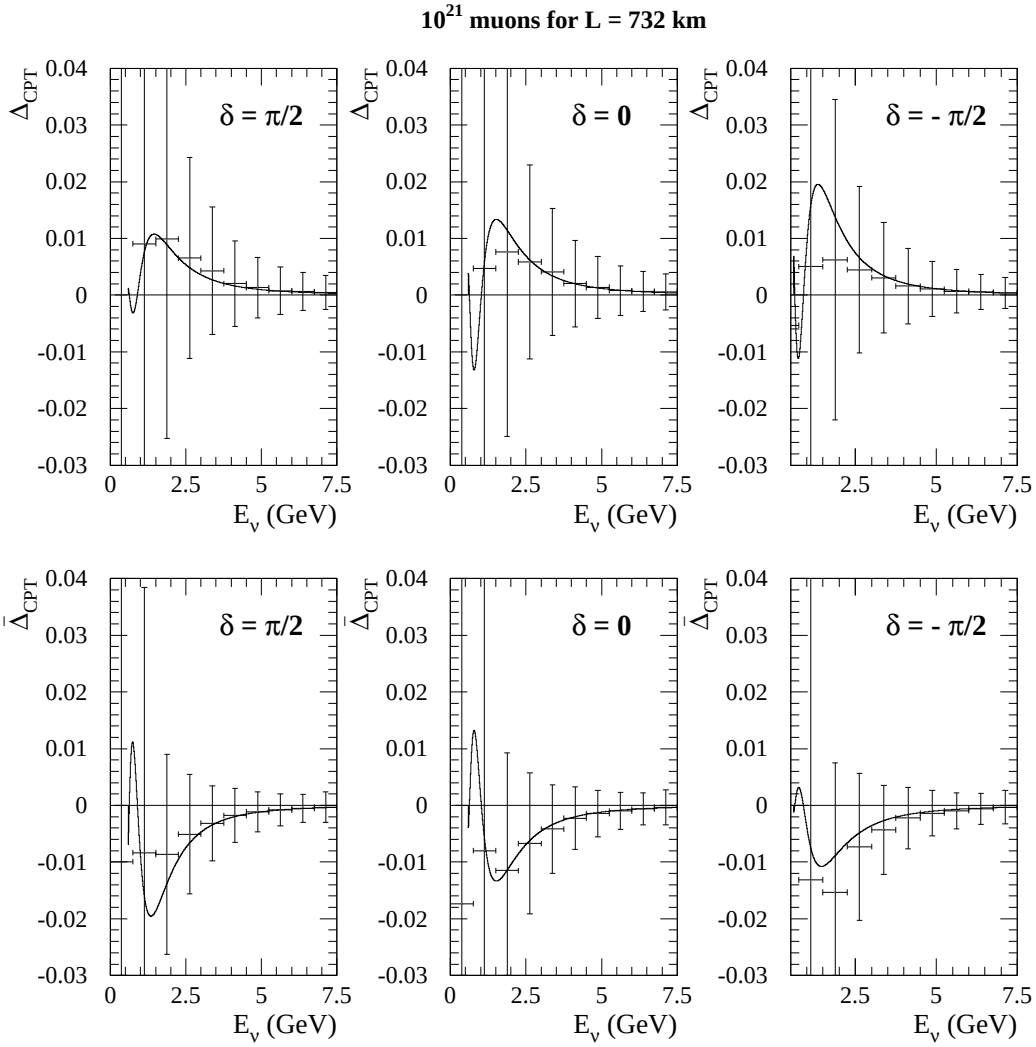

Figure 19: Direct CPT-violation: Binned $\Delta_{CPT}(i)$ (upper plots) and $\bar{\Delta}_{CPT}(i)$ (lower plots) for three values of the δ-phase: $\delta = +\pi/2$, $\delta = 0$ and $\delta = -\pi/2$. The errors are statistical and correspond to a normalization of 10^{21} muon decays and a baseline of $L = 732$ km. A 20% electron efficiency with a charge confusion probability of 0.1% has been assumed. The change of sign of the effect with respect to the substitution of neutrinos by antineutrinos is clearly visible. The full curve corresponds to the theoretical probability difference.

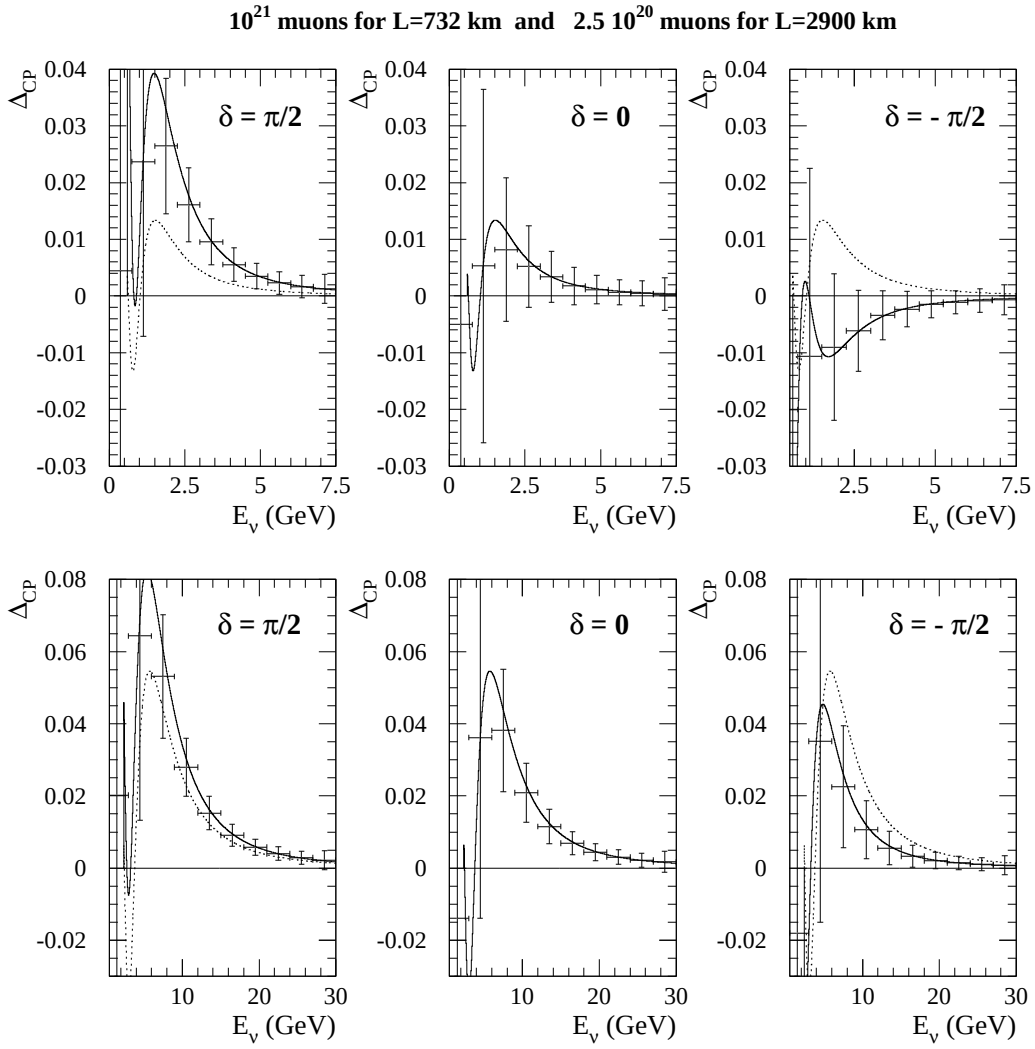

Figure 20: Direct CP-violation: Binned $\Delta_{CP}(i)$ discriminant for the shortest baseline $L = 732$ km, $E_\mu = 7.5$ GeV (upper plots) and longest baseline $L = 2900$ km, $E_\mu = 30$ GeV (lower plots) for three values of the δ-phase: $\delta = +\pi/2$, $\delta = 0$ and $\delta = -\pi/2$. The errors are statistical and correspond to a normalization of $10^{21}(2.5 \times 10^{20})$ for $L = 732(2900)$ km. The full curve corresponds to the theoretical probability difference. The dotted curve is the theoretical curve for $\delta = 0$ and represents the effect of propagation in matter.

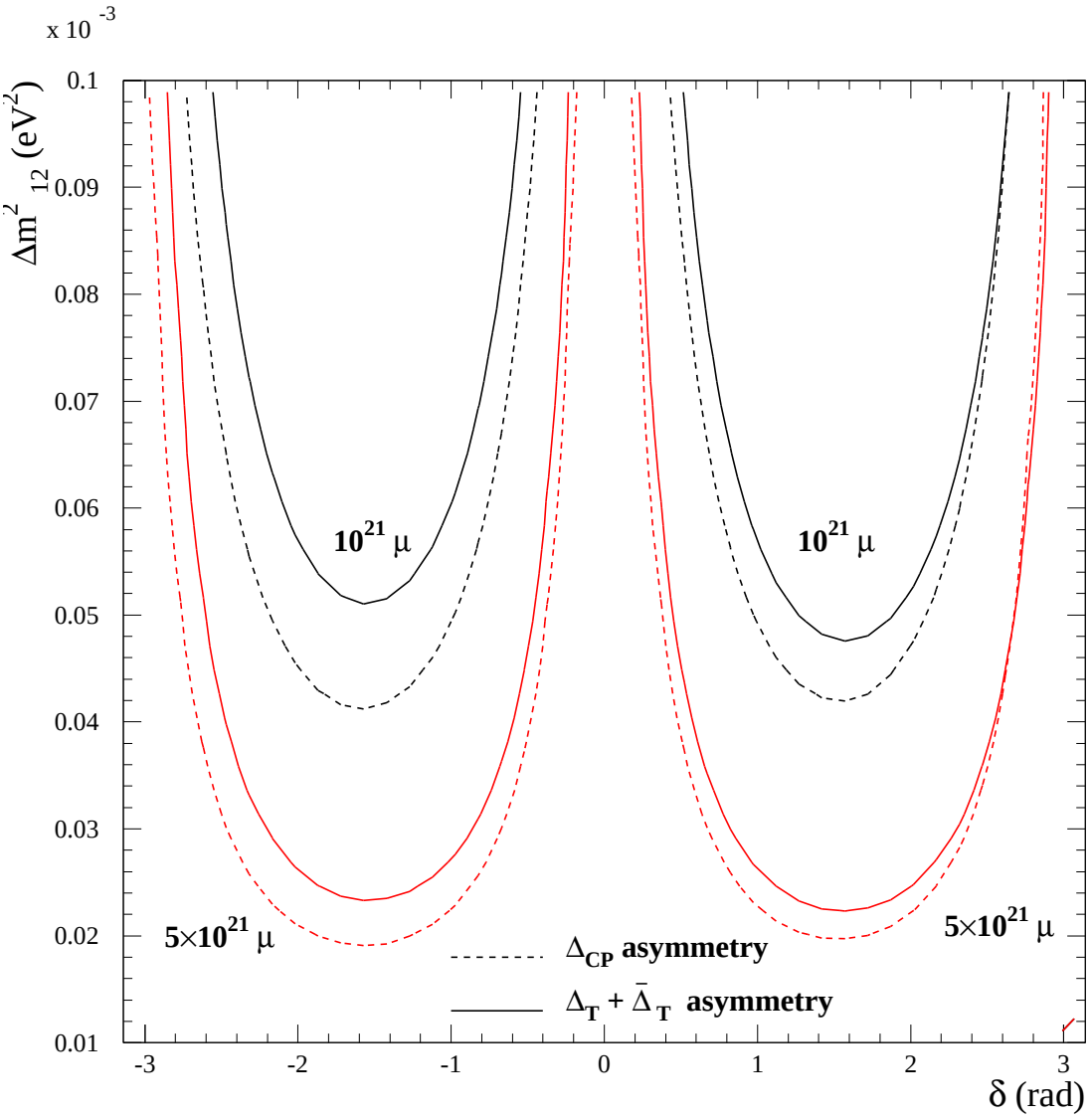

Figure 21: Exclusion region at the 90%C.L. ($\chi^2 > \chi^2_{min} + 1.96$) in the δ-phase vs Δm^2_{21} plane. Two regions obtained with the Δ_{CP} and the sum of Δ_T and $\bar{\Delta}_T$ discriminants are shown. A charge confusion probability of 0.1% and an electron efficiency of 20% has been assumed. The result is shown for two normalizations, 10^{21} and 5×10^{21} muon decays of each type with energy $E_\mu = 7.5$ GeV and a baseline of $L = 732$ km. The reference oscillation parameters are $\Delta m^2_{32} = 3 \times 10^{-3}$ eV^2, $\sin^2\theta_{23} = 0.5$, $\sin^2\theta_{12} = 0.5$ and $\sin^2 2\theta_{13} = 0.05$.

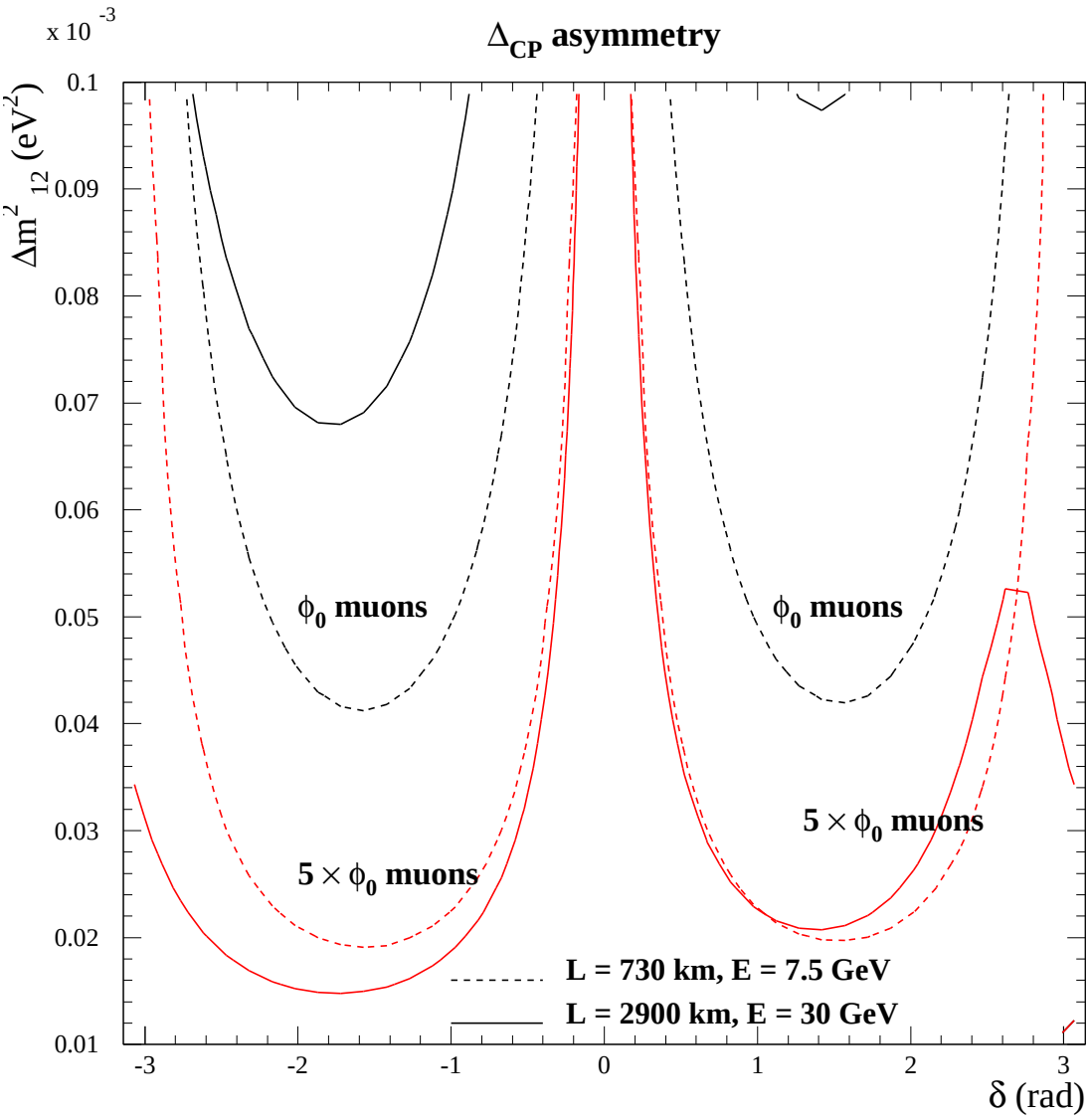

Figure 22: Exclusion region at the 90%C.L. ($\chi^2 > \chi^2_{min} + 1.96$) in the δ-phase vs Δm^2_{21} from the Δ_{CP} discriminant. The result is shown for two baselines and two normalizations: ($L = 732$ km, $E_\mu = 7.5$ GeV, $\phi_0 = 10^{21} \mu$ flux) and ($L = 2900$ km, $E_\mu = 30$ GeV, $\phi_0 = 2.5 \times 10^{20} \mu$ flux). The reference oscillation parameters are $\Delta m^2_{32} = 3 \times 10^{-3}$ eV^2, $\sin^2 \theta_{23} = 0.5$, $\sin^2 \theta_{12} = 0.5$ and $\sin^2 2\theta_{13} = 0.05$.

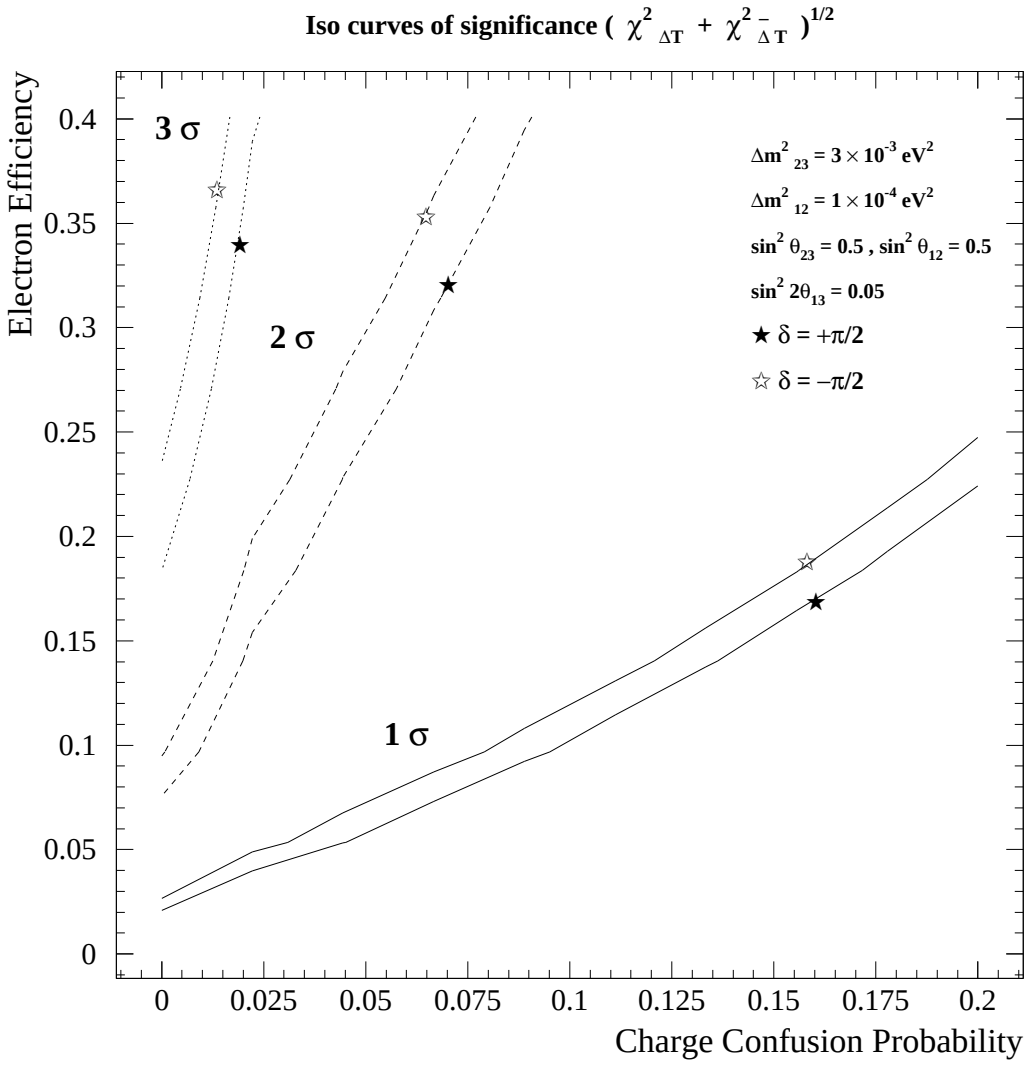

Figure 23: The 1σ, 2σ and 3σ χ^2 contours of the combined Δ_T and $\bar{\Delta}_T$ discriminants as a function of the electron efficiency and the probability for charge confusion. The result is shown for $\delta = +\pi/2$ and $\delta = -\pi/2$. The other oscillation parameters are $\Delta m^2_{32} = 3 \times 10^{-3}$ eV^2, $\Delta m^2_{21} = 1 \times 10^{-4}$ eV^2, $\sin^2 \theta_{23} = 0.5$, $\sin^2 \theta_{12} = 0.5$ and $\sin^2 2\theta_{13} = 0.05$.

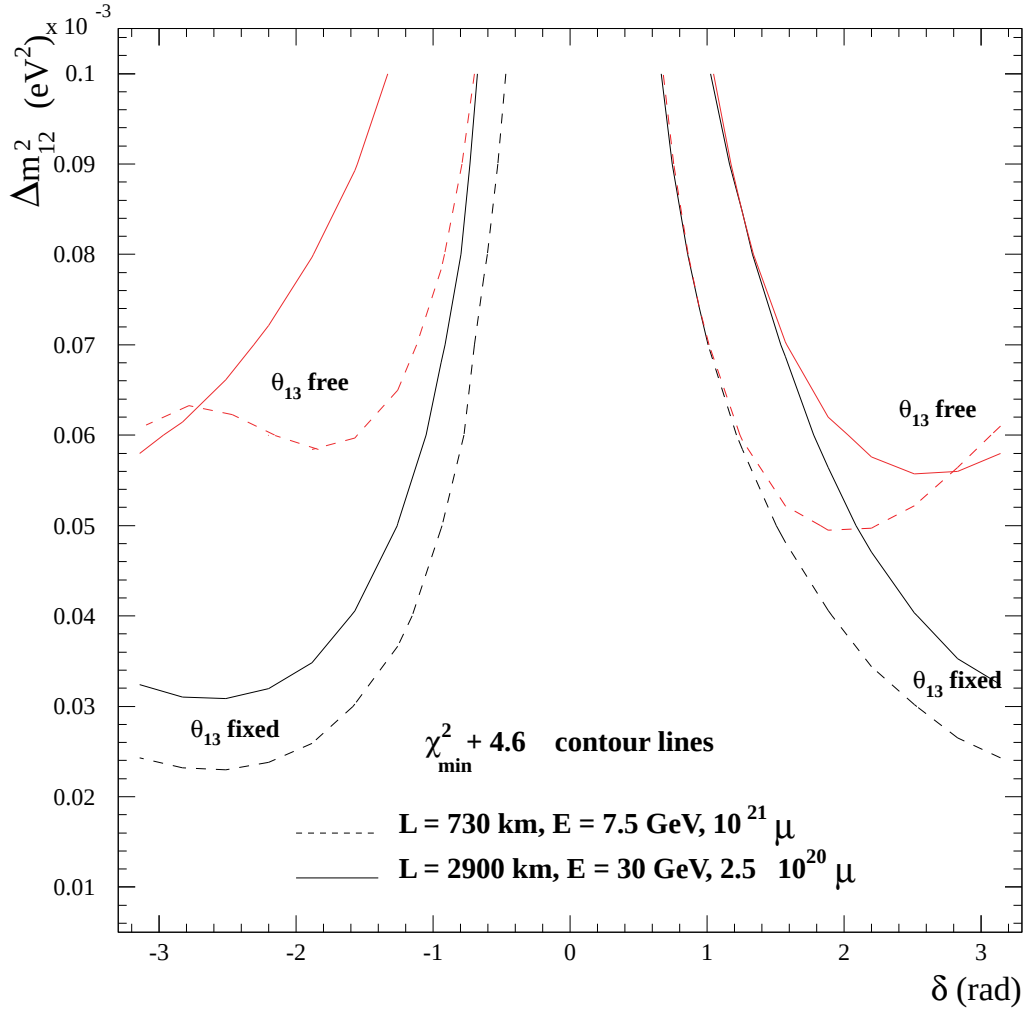

Figure 24: 90% C.L. sensitivity on the CP-phase δ as a function of Δm^2_{21} for the two considered baselines. The reference oscillation parameters are $\Delta m^2_{32} = 3 \times 10^{-3}$ eV^2, $\sin^2\theta_{23} = 0.5$, $\sin^2\theta_{12} = 0.5$, $\sin^2 2\theta_{13} = 0.05$ and $\delta = 0$. The lower curves are made fixing all parameters to the reference values while for the upper curves θ_{13} is free.